# Reverse Frequency Allocation Schemes in Heterogeneous Networks


By

Aneeqa Ijaz

**NUST201464051MSEECS61214F**

Supervisor

**Dr. Syed Ali Hassan**

**Department of Electrical Engineering**

A thesis submitted in partial fulfillment of the requirements for the degree of Masters of Science in Electrical Engineering (MS EE)

In

School of Electrical Engineering and Computer Science,

National University of Sciences and Technology (NUST),

Islamabad, Pakistan.

(January 2017)

# Approval

It is certified that the contents and form of the thesis entitled "**Reverse Frequency Allocation Schemes in Heterogeneous Networks** " submitted by Aneeqa Ijaz have been found satisfactory for the requirement of the degree.

Advisor: **Dr. Syed Ali Hassan**

Signature: _____

Date: _____

Committee Member 1: **Dr. Sajid Saleem**

Signature: _____

Date: _____

Committee Member 2: **Dr. Fahd Ahmed Khan**

Signature: _____

Date: _____

Committee Member 3: **Dr. Rizwan Ahmad**

Signature: _____

Date: _____

# Abstract

Addressing the enormous growth of mobile data traffic becomes the key driving force for the evolution of 5th generation (5G) networks. The ever increasing demand of data rates can no longer be fulfilled by the conventional macro cellular network. With exponential proliferation of smart phones, augmented reality (AR) applications are gaining huge momentum, possibly rendering AR as killer application for next generation of cellular network. To summarize two key requirements which have emerged from various verticals for future wireless networks are low latency and higher throughput. Keeping this in mind both academia and industry are currently working on developing fifth-generation (5G) wireless networks. 5G wireless networks are geared to exploit aggressive spatial reuse of spectrum to realize higher throughput via heterogeneous cellular architecture, i.e., HCNs (heterogeneous cellular networks). However deployment of HCNs still has to face many challenges such as expensive hardware, increased complexity and performance degradation due to several sources of interference. The core ambition of this work is to provide elevated data rates and better coverage to the downlink users. In this thesis a variant of shared frequency scheme, reverse frequency allocation scheme (RFA) has been exploited that avoids the prominent source of interference by

partitioning the macro cell into non overlapping regions and applying complementary spectrum allocation between the macrocells and picocells. By employing well known tools from stochastic geometry we derived closed-form expressions for the coverage probability and rate coverage in two tier cellular network employing RFA and its variants. The modeling is performed using two approaches; one where the BSs and users are modeled as independent Poisson point process (PPP) and in the second approach, the interference is approximated using the fluid model.

# Dedication

To my parents and teachers.

# Certificate of Originality

I hereby declare that this submission is my own work and to the best of my knowledge it contains no materials previously published or written by another person, nor material which to a substantial extent has been accepted for the award of any degree or diploma at NUST SEECS or at any other educational institute, except where due acknowledgement has been made in the thesis. Any contribution made to the research by others, with whom I have worked at NUST SEECS or elsewhere, is explicitly acknowledged in the thesis.

I also declare that the intellectual content of this thesis is the product of my own work, except for the assistance from others in the project's design and conception or in style, presentation and linguistics which has been acknowledged.

Author Name: Aneeqa Ijaz

Signature: _____

# Acknowledgment

I am thankful to Almighty Allah, it would not have been possible without His blessings. I am eternally thankful to my family who have always supported me and motivate me during the entire duration of dissertation. I am very grateful to Dr. Syed Ali Hassan, without his persistent guidance and support I could not be able to complete my research work. It's his quick and constructive feedback that kept me going during the journey, its truly an honor working with such a dedicated and helpful supervisor.

# Table of Contents

# List of Figures

# List of Tables

# Chapter 1

# Introduction

Meeting the exponential increasing demands of higher data traffic is one of the momentous challenges. It is required that the existing infrastructure should be revived because the spectrum is limited and the demand of services is increasing drastically. Wireless cellular networks mainly based on two technologies, the wireless cellular networks (WCNs), in which users get voice services along with high mobility and wireless local area networks (WLANs) that provide communication services to the users with higher throughput but at the cost of restricted mobility. It is expected that both these technologies should take over their shortcomings and make the services possible every where along with mobility and better data rates. The recent forecast in [1], the mobile data traffic would be increased by 1000 folds from 2010 to 2020 and probably 10,000 times by 2025. Exponential increase of load has become a cause of macro cellular network congestion and as a consequence, the performance of wireless systems degrade immensely. Therefore, the cellular network is under the continual phase of transition, in order to deploy a com-

plementary solution that can ease the burden of macro base stations. In 2010, ITU approved two technologies as 4G candidates, LTE advanced and IEEE 802.16m. IEEE 802.16m is an improved version of IEEE 802.16e/Mobile WiMax and LTE-Advanced is an upgraded version of already existing LTE technology. The main goals of LTE advanced are higher coverage especially at cell edge, better throughput using relay nodes, low interference that is achieved through CoMP that enables to exchanges the data among several base stations simultaneously.

Futhermore, this unprecedented demand for wireless connectivity is increasingly becoming heterogeneous due to considerable need for connecting machines with other machines paving way for Internet-of-Things. To summarize, the two key requirements which have emerged from various verticals for future wireless networks are low latency and higher throughput. Keeping this in mind both academia and industry are currently working on developing fifth-generation (5G) wireless networks. The primary goal of 5G is to provide high speed internet to the mobile users, enhanced coverage to more number of users per unit area and unlimited data rates. To facilitate the subscribers with better services 5G has been complemented with many other distinctive attributes such as heterogeneous cellular networks (HCNs), millimeter wave (mmWave) communications, massive multiple-input multiple-output (MIMO), and other multiple access schemes to give the additional boost in the data rates and improving the coverage range.

Despite of the potential advantages of these above mentioned techniques, each technology have some challenges in its deployment. For instance, although HCNs incorporate access points of several tiers, however dealing with

the cross-tier as well as co-tier interference such that the required SINR remains greater than the given threshold and to provide bandwidth fairness among the users of different tiers is a difficult challenge [2]. mmWave communications can be performed at higher frequencies (30 and 300 GHz) and it is expected that they can cater 200 times greater than all cellular allocations [16]. But mmWave are subjected to high penetration loss, due to smaller wavelength they do not diffract well and they have smaller value of SINR values additional loses from the blockage can not be tolerated. Whereas Massive MIMO deployment faces coupling effect, pilot contamination due to faulty channel estimation [3].

Therefore, the real challenge is to exploit the benefits of these new emerging techniques while coping with the drawbacks such that we can get maximum benefit out of it in terms of higher data rates, coverage, planning ease of use ,scalability, mobility, and quality of service. Higher data rates can be achieved when the provided signal-to-interference plus noise ratio (SINR) is greater than a pre-defined threshold. This could be possible when the moving subscriber is within the range of the base station and away from the interfering entities. In addition, the Capacity can also be elevated by utilizing orthogonal access schemes, frequency reuse schemes, cell sectoring and cell splitting are also proved to be the workable solutions that enhance the SINR values.

## 1.1 Heterogeneous Cellular Networks (HCNs)

Generally, outdoor users receive the SINR greater than the required threshold, however, the signal quality degraded immensely in an indoor environment. And it is expected that as the data traffic increases, the origin of more than 70% of this traffic will be from indoor but the subscribers can not solely depend upon the services from the outdoor transmitting BSs that are installed at quite higher altitudes. Due to the high penetration losses, the signals from the distant located BSs become attenuated leading to the lower data rates. To encounter this problem we can install more macro BSs but this solution is very expensive in term of cost, planning and optimization as well. Another solution is the deployment of small cells, the eminent advantage of SAPs is that they can be seamlessly overlaid in the existing macro cellular wireless networks, whereby due to the successful deployment according to [4], the number of small base stations (SBSs) would increase upto 17 million by 2017. Since small cell is an umbrella term for operator controlled low powered base stations of several sizes and different coverage range, like femto cell, Pico cell and micro cells as depicted in Figure 1. Some of the attributes of small cells are as following:

- **Femto cells:**Femto cells have a coverage area of 10 to 100 m and when they are used indoor they are known as eNBs for LTE. They have a size of home router and its deployment is increase tremendously from the past few years as they can be easily installed by the subscribers [6].

- **Pico cells:**They have the ability to support almost 100 users with in

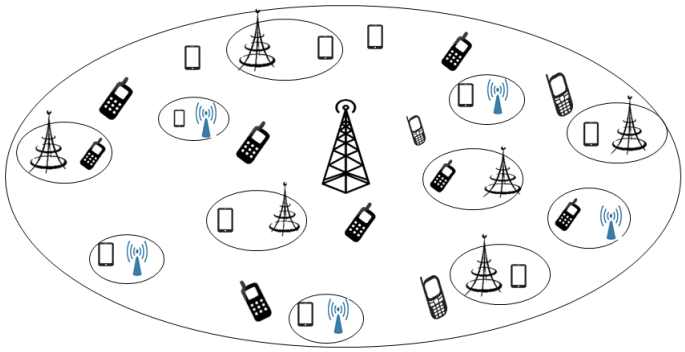

Figure 1.1: Hetrogeneous cellular network comprises of three tiers

the coverage area of 100 to 200 meter. They are similar to that of femto cell but the difference lies in the range, higher data rate more user to serve in a given area and deployed by the operators. They have GPRS gateway to communicate with the neighboring cells. The enterprise small cell network (E-SCN) have multiple copies of the access point of Pico cells. ESCN combine all the signals from the copies of Pico cell and generate a single stream of signal [7].

- **Micro cells**:These cells have a greater coverage compared to the rest of above mentioned two cells. They have a coverage area of 200 to 2000 meters and can provide services to up to 2000 users lies with in the given area. Even they can be used in the outside environment as a replacement where macro cell cannot provide enough coverage [8].

These BSs of various tiers included in HCNs vary in their transmit power, density, coverage range and signal-to-interference plus noise ratio (SINR) thresholds. Therefore, user experience in terms of rate, reliability and coverage is varying as compared to the stand alone macro BS networks. Some of

the prominent attributes of dense small cell networks are

- Can provide better coverage mostly indoor but Pico cells can also provide good outdoor coverage.
- As small cell network utilizes less power so their battery life is very good and they can be proved as energy efficient solution.
- Can reduce the load of macro cell base station in hotspot areas by providing coverage to the users with in its own area.
- As the distance between the small cell and the subscriber is of few meters, therefore there is less power loss and lower level of interference.

Moreover, they can operate in several modes such as open, closed, or hybrid access mode. In an open access strategy, the users can connect to the BS of any tier available in the network that provides the highest reference signal received power (RSRP). In closed access mode, the subscribers are allowed to connect to a particular tier, where the remaining tiers are considered as interferers [9]. However, in hybrid access policy [10, 11], the operator can restrict the connection of users to the access points (APs) of specific tiers. The selection of access policy depends upon the network requirement, which is a tradeoff between bandwidth availability and interference avoidance.

## 1.2 Motivation

Deployment of hetnets is a very proficient solution but mostly users prefer to connect to the MBS mking BSs highly congested, offloading the traffic

and directing it towards the small access points and providing coverage to the indoor users is a crucial task. Deployment of picocells along with the macro cells has lead to further challenges, for instance, adding heterogeneity in network architecture gives rise to incremental complexity in the analysis and modeling of cellular networks. Secondly, it is quite a laborious task to deal with the cumulative effect of interference from different tiers and from the cells of same tier while evaluating the SINR and throughput of the mobile users. Hence, this stands as a necessity to consider for a pragmatic solution that not only minimizes the impact of co-tier and cross-tier interference but also provides phenomenal boost in the data rates. Many frequency allocation schemes has been proposed to completely avoid the interference that provide separate bands to each tier but that decline the data rate severely other schemes provide the access of entire band to the macro users but the users attached to SAPs have to wait for their turn so that they do not cause interference in the transmission of macro users in this way the users suffer. Another scheme is to provide the whole spectrum to both macro users as well as the pico users this scheme is good for the rates but the question of how to deal with this interference becomes the main issue. In this thesis we proposed a variant of shared frequency allocation scheme that can avoid strong sources of interference by dividing the cells and users into regions and reverses the transmission direction of both the tiers, eventually enhance the performance of the network in terms of coverage and data rates.

## 1.3 Problem Statement

The objective of this thesis is to provide an innovative frequency allocation scheme, that has low complexity, overhead and also provide eminent degradation in the interference both co-tier as well as cross-tier. Consequently, better data rates are provided to the downlink small cell users. To evaluate the network performance closed-form mathematical expressions for coverage probabiltiy and rate coverage are derived that capture the important metrics like SINR, coverage probability, average rates and outage capacity.

## 1.4 Contribution

The main contribution of this thesis is as follows:

- We considered a variant of shared frequency scheme in which the users get lower interference by dividing the cells into higher regions and proved that after partitioning up to certain region the outage probability becomes saturated.

- By simply dividing the cell we can achieve better SINR and eventually better coverage is attained, however, the data rates decrease, therefore we devise a combination of RFA schemes that take advantage of useful aspects of several RFA scheme and proposed and optimal modified RFA scheme. We also give insights that partitioning the macrocell into more and more regions is not a practical solution and after certain divisions saturation occurs and analyze the performance of network in terms of outage probability, sum rate and outage capacity

- We then formulated a stochastic geometry based analysis in which the distribution follow either independent homogenous PPP or uniform distribution and derive the closed-form expressions for multiple region RFA scheme in terms of coverage probability and coverage rate.

## 1.5 Thesis Organization

The rest of the thesis organization: In Chapter 2 literature review of some of the spectrum allocation schemes along with some interference mitigation and traffic adaption (IMTA) techniques are discussed. Chapter 3 presents the system model of RFA scheme in the multi cell multi region and also the combination of RFA schemes that devise modified RFA schemes. In Chapter 4 we propose the stochastic geometry based frame work in which the users and femto cells having Poisson point process distribution and derived the closed form expression for the coverage as well as the rate analysis. Chapter 5 will discuss the simulation results and their matching with the analytical expressions. Finally, Chapter 6 provides the conclusion and the future work.

# Chapter 2

# Literature Review

The idea of heterogeneous networks (HetNets) has been proposed in 3rd Generation Partnership Project (3GPP) and coined forward as a potential candidate for fifth generation (5G) communications. where small cells are deployed along with the existing macro cellular network and both utilize the same licensed spectrum. HCNs are efficient as well as cost effective solution for offloading the mobile users from the macro base station to small access points (SAPs). SAPs include operator and/or user deployed pico base stations (PBSs) [19], or femto BSs [20, 21], provisioned with multiple radio access technologies (multi-RAT). The BSs of various tiers included in HCNs vary in their transmit power, density, propagation characteristics (e.g., path loss exponents), deployment modes (e.g., open vs. closed, indoor vs. outdoor) and supported quality of service (QoS) requirements. Therefore, user experience in terms of rate, reliability and coverage is varying as compared to the standalone macro BS networks. Some recent results of deploying HetNets with and without millimeter spectrum are discussed in [12–15]. The

eminent advantage of SAPs is that they can be seamlessly overlaid in the existing macro cellular wireless networks whereby according to [5], the number of small base stations (SBS) would increase upto 17 million by 2017. As the number of tiers is increased to improve the performance of the wireless network, the system has to face major technical challenges, for instance, dealing with the aggregate effect of interference from different tiers and from the cells of same tier while evaluating the signal-to-interference plus noise ratio (SINR) and throughput of the mobile users, increased complexity, self organization, backhauling and handover etc. Hence, this stands as a necessity to consider for a pragmatic solution that not only minimizes these challenges but also provides phenomenal boost in the data rates. Interference can be reduced with in the operator deployed macrocells by implementing interference management techniques such as the frequency reuse schemes, sub-carrier allocation, codebook restriction strategy to select the best channel [22], and centralization of the network. However, these techniques can be deployed in co-tier cellular network. For the intercell interference (ICI) management in HetNets, 3GPP Release 10 introduced almost blank sub-frames (ABS)/ based enhanced inter cell interference coordination (eICIC) which is an efficient way to increase the cell-edge area of users [23]. Reducing the power of the small cells increases the throughput of the victim macro user equipments (MUEs) [24], and efficiently defining the user association criteria also enhances the performance of HetNets [25].

A number of recent literature addressed the main issues of interference, limited resource availability and load balancing thereby introducing the schemes that mitigate interference in heterogeneous cellular networks [26], improve ca-

pacity by using the spectrum resources efficiently [27] and by offloading the traffic towards SAPs [28, 29]. Other solutions include power control mechanism, adjusting the transmissions of both tiers in separate time frames for achieving significant gain in the data rates. To mitigate the impact of interference, we present an efficient frequency allocation scheme in a two tier network that reverses the transmission direction of both tiers, thereby enhances the data rates of downlink users. The following subsection gives an overview of relevant literature in HetNets.

## 2.1 Related work and Motivation

In the architecture where the users are allowed to connect to the APs of any tier, they generally connect to high powered macro base stations (MBSs), causing the load disparity and under utilization of resources. On the other hand, for load balancing, MBS can offload small fraction of macro users to SAPs, however, this leads to lower SINR. Therefore, during the transmission/ reception period of small cells, the time/frequency resources of the macro cells become mute [30], leading to the wastage of time/frequency resources assigned to the subscribers attached to the MBS. Moreover, for load balancing, only a limited number of users can be offloaded to the SAPs and the users connected to the SAPs do not receive optimal SINR. Therefore, it is required to apply some resource allocation algorithm along with innovative interference mitigation schemes to substantially enhance the gains of the network.

In [27], many frequency allocation schemes are discussed to minimize the

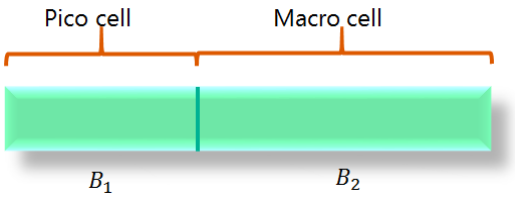


Figure 2.1: Static fractional frequency reuse scheme.

impact of interference and fair resource partitioning among the users connected to macro cells and femto cells. A comprehensive survey [31], depicts many strategies to deal with the interference scenarios. In [32], buffered fractional frequency reuse (FFR) scheme for the elevation of data rates of cell edge macro user equipments (MUEs), is developed and compared with several other frequency reuse schemes. A detailed analysis of coverage probability for open and closed access modes for FFR schemes is proposed in [33]. Universal blanking pattern is introduced in [34] to provide coordination among base stations of various tiers and reducing interference by using physical resource block allocation. The performance and spectral efficiency of SAPs can be improved by utilizing antennas selection diversity schemes and beamforming for interference management in uplink as well as in downlink [35]. A variant of shared frequency scheme is proposed in [36] that avoids the prominent source of interference from MBS by dividing the macrocell into several regions. In [41], a cross-polarized complementary frequency allocation (CPCFA) scheme in femto-macro networks is introduced to exploit the diversity in the frequency spectrum by employing the cross-polarization discrimination (XPD) property that supports the independent operations within each of the tier by utilizing different polarizations at the cost of complexity.

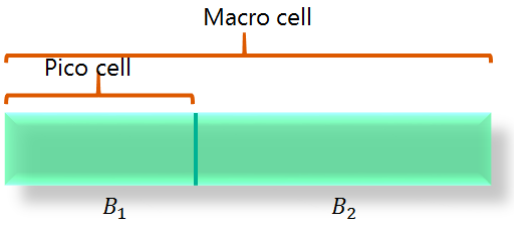


Figure 2.2: Sub-band frequency reuse scheme.

## 2.2 Frequency Allocation Schemes

To mitigate the impact of interference, several frequency allocation schemes have also been proposed in [37–39] including static, dynamic, sub-frequency band and shared frequency reuse strategies. In static frequency reuse scheme, there are dedicated frequency bands for picocells and macrocells [37], as can be seen in Fig. 2.1, which leads to the wastage of resources that are already scarce. Whereas, in sub-band frequency reuse scheme the macro tier is allowed to use the entire band and small cell users are allowed to use the small dedicated spectrum, depicted in Fig. 2.2, causing severe interference. As the users connected to the small access points already receive lower received power from low powered BSs and the signal becomes further attenuated due to high powered MBS, thus the data rates of the users also decrease. In dynamic frequency allocation scheme, the overall traffic is being monitored by the continuous signaling between the two tiers and the spectrum is allocated dynamically. Thus, dynamic frequency reuse scheme behaves spectrum efficient as compared to static scheme, but at the cost of higher complexity and persistent signaling [38]. In shared frequency band scheme, the whole spectrum is utilized by the two tiers, which provides the most spectral efficient solution at the expense of strong interference [41]. The shared frequency

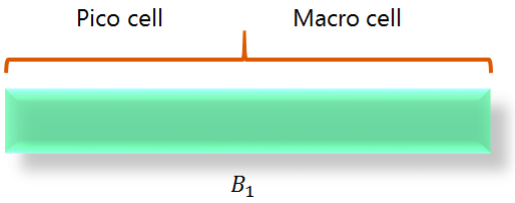


Figure 2.3: Shared fractional reuse scheme.

band scheme generally results in user fairness for both macro as well as pico users because the entire spectrum is available to both tiers, with no particular priority and signaling, shown in Fig. 2.3. However, because of simultaneous transmissions in both tiers, the cross-tier interference becomes a major concern. Therefore, many frequency allocation scheme for the efficient resource utilization are devised to minimize the impact of interference and enhance the data rates.

## 2.3 Variants of shared frequency allocation scheme:

### 2.3.1 FFR:

Strict fractional frequency reuse (FFR) scheme is proposed [39], in which the cell is partitioned into two regions. A frequency reuse factor (FRF) of unity is applied to the cell center region while higher values of FRF are assigned to the cell edge region. In a multi-cell scenario, the cells in a cluster share the same frequency band in their center region while the cell edge regions have the remaining dedicated frequency bands but this scheme is spectrally not very efficient. As can be seen in Fig. 2.4, same band is assigned to the

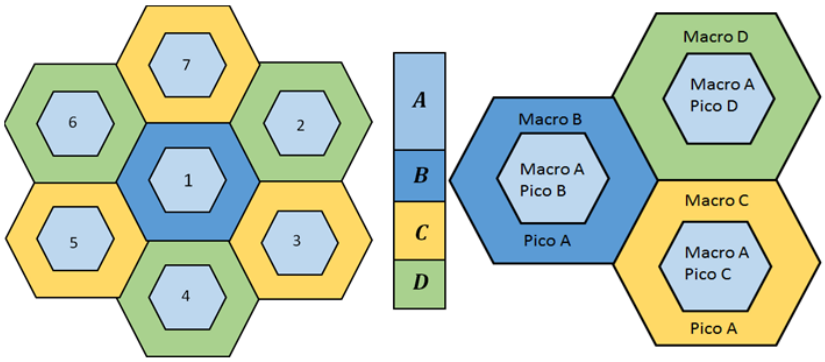


Figure 2.4: Fractional frequency reuse scheme.

cell center regions of all the cells of cluster, where as frequency reuse factor of 3 is used at the cell edge regions of neighboring cells of the cluster. Thus it can be said that a total of N+1 sub-bands are required for the deployment of this scheme. In the figure the whole spectrum is divided into 4 sub-bands. As the cell edge users are not allowed to use the band that the users of cell center region are using, therefore the impact of interference is low, however the users of both regions do not get high enough throughput.

### 2.3.2 SFR:

Another relatively efficient scheme is the soft fractional frequency reuse (SFR) that is similar to the strict frequency reuse scheme but in this case, the users of both regions havethe access to full spectrum [40]. For instance, if a frequency band is divided into 3 sub-bands, the central region macro users utilize $1/3^{rd}$ of the spectrum and $2/3^{rd}$ will be allotted to the pico users. On the other hand, opposite phenomena is implemented in the cell edge region, i.e., the macro users will have $2/3^{rd}$ of sub-carriers and $1/3^{rd}$ of the frequency band is allocated to the pico users, as depicted in Fig. 2.5. Additionally, in-

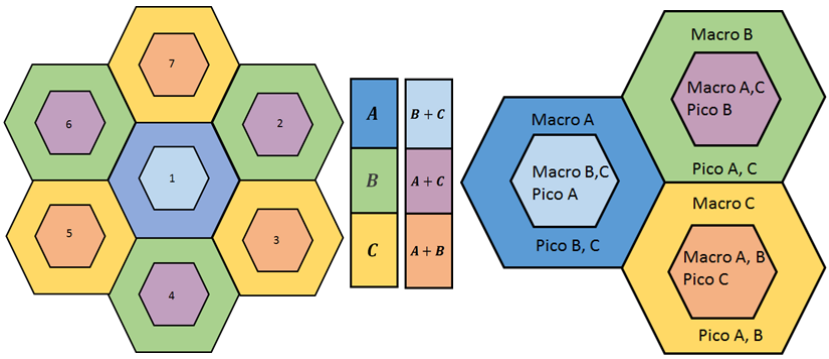


Figure 2.5: Soft fractional frequency reuse scheme.

terference is being controlled by applying power allocation, i.e., if the user is located in the cell center region the SAPs transmit with less transmit power, whereas as for cell edge users this power is higher.

Motivated by the results of [36], in this thesis, we deploy a variant of shared frequency scheme, namely reverse frequency allocation (RFA) in a dense heterogeneous network comprising of two tiers, i.e., picocells and macrocells. We present a framework based on the stochastic geometry that analyzes the coverage of users attached to the pico BSs in a closed subscriber group (CSG). RFA scheme provide significant gains in the data rates of downlink pico user equipments (PUEs) by partitioning the cell into non-overlapping regions and applying complementary spectrum allocation between the macrocells and picocells, i.e., the direction of radio transmissions of macrocells is reversed and allocated to the picocells that are in the other spatially separated area. Hence, there is a prominent reduction in the number of interfering cells in each region of a macro cell, whereas the detrimental effect of MBS interference is completely avoided.

# Chapter 3

# Reverse Frequency allocation Scheme in HetNets

In this thesis we present a novel variant of shared frequency scheme known as reverse frequency allocation (RFA) scheme, which addresses the spectrum sharing challenge and enhances the data rates of downlink PUEs. In RFA, the cell is partitioned into non-overlapping regions and the basic idea is to introduce the complementary spectrum allocation between the macrocells and picocells, i.e., the direction of radio transmissions of macrocells is reversed and allocated to picocells that are in the other spatially separated area. This potentially reduces the number of interferers and also the prominent interference from the MBS is entirely avoided. In [41], two region RFA is implemented on multi-cell, however, the neighboring cells caused a great source of interference whereas in [36], multiple region RFA in a single cell has been simulated, however, this work did not consider the problem of inter cell interference (ICI). We accumulate the aspects of previous works and devise a

multi-dimensional model of a multi-cell multiple region RFA to enhance the data rates of the network.

## 3.1 Frequency Allocation in 2-RFA

Like other FFR schemes (SFR), a conventional 2-RFA scheme [42] divides the coverage area of each macrocell into two regions, i.e., an interior region and an exterior region [43]. However, distinguished attribute in this scheme is the reversal of transmission directions of the two tiers to achieve minimal interference and maximum gain for the downlink (DL) users. Furthermore, frequency division duplexing (FDD) scheme is considered, where the traffic in this study is assumed to be symmetrical and equal bandwidth, $b_{ul}$ is allocated for the uplink transmission and downlink $b_{dl}$ channels, i.e., $B = b_{dl} \bigcup b_{ul}$, where $B$ is the available bandwidth. Additionally, there exist no interference between UL and DL traffic of the same tier. Taking advantage of this aspect, the downlink (DL) frequency spectrum of inner region PUEs is allocated to the uplink (UL) outer region MUEs and the uplink frequency band of the inner PUEs is allocated to the outer region downlink MUEs. On the other hand, the outer UL frequency band of PUEs is allocated to the inner DL MUEs and the outer DL sub-band of PUEs to the inner UL MUEs. On a side role, soft frequency reuse strategy allocates spectrum in such a manner that the DL PUEs have to face strong interference from the MBS whereas in RFA, the PUEs encounter cross-tier interference from low-powered MUEs only, which reduces the level of interference to a considerate amount. When we evaluate the system from the downlink perspective, RFA scheme provides

Table 3.1: Frequency Distribution in 2-RFA Scheme.

| $B_1$ | | $B_2$ | |
|---|---|---|---|
| | | | |
| Inner UL Picocell | Inner DL Pico cell | Outer UL Picocell | Outer DL Picocell |
| $B_{1x}$ | $B_{1y}$ | $B_{2x}$ | $B_{2y}$ |
| Outer DL Macrocell | Outer UL Macrocell | Inner DL Macrocell | Inner UL Macrocell |

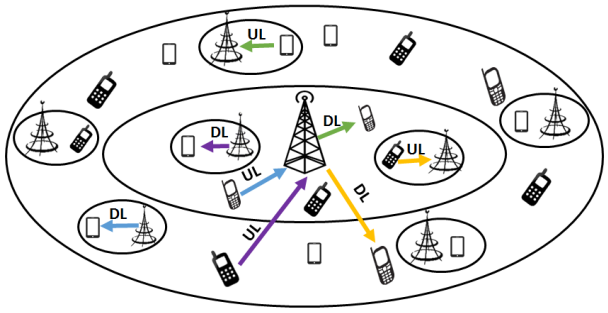


Figure 3.1: Illustration of 2-RFA in a single cell with two-tier network.(The signaling colors are conversant with the spectrum colors in the Table 3.1)

lower cross-tier interference, hence better signal-to-interference plus noise ratio (SINR) is achieved. The frequency allocation for 2-RFA is shown in Table 3.1.

The downlink SINR of the PUE attached to the serving PBS in the any region of a single cell is formulated as

$$SINR = \frac{P_p h_i ||x_i||^{-\beta_2}}{\Sigma_{q=1,q\neq i}^{\Psi} P_p h_q ||x_q||^{-\beta_2} + \Sigma_{m=1}^{\Omega} P_m h_m ||x_m||^{-\beta_1} + \sigma^2}, \tag{3.1}$$

where $P_p$ and $P_m$ are the transmission power of PBSs and MUEs, respectively, $h_i \sim$ exp(1) is independently and identically distributed (i.i.d) exponential fading gain with unit mean. The path loss function is expressed as $||x_i||^{-\beta_2}$, where $x_i$ is the distance between the intended PUE and the serving PBS, $\beta_2$ is the path loss exponent for the pico tier and $\beta_1$ for macro tier. The

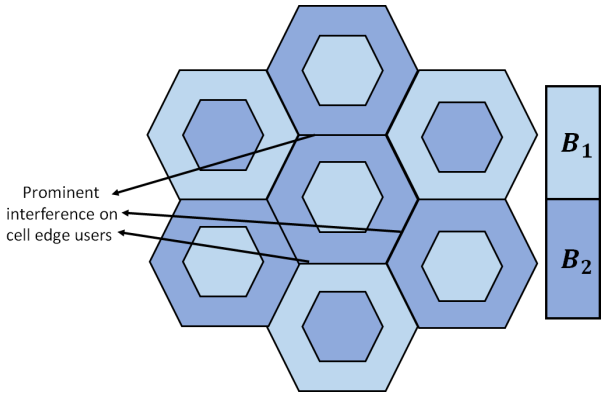


Figure 3.2: 2-RFA in a multi-cell scenario. The cell area is divided into two regions with frequency bands $B_1$ and $B_2$.

denominator of (1) represents the interference that PUE experiences from all the DL PBSs $\Psi$ located in the same region other than the serving PBS and from the UL MUEs $\Omega$ in any other region exploiting same bandwidth spectrum, respectively, while $\sigma^2$ shows the noise power. This is due to the fact that RFA scheme reverses the direction of transmitting frequencies, thus, any interference from MBS is prohibited, which otherwise is a prominent source of degradation of SINR. Extending the concept of 2-RFA in a multi-cellular network, it is evident that the interference management becomes a difficult task as the number of interferers increases drastically and the ICI for outer region femtocells becomes inevitable. Fig. 3.2 depicts the multi-cell 2-RFA scheme, and it shows the interference during the downlink transmission would increase many folds due to the direct obstruction from closely attached 3 macrocells, badly affecting the cell edge users [41]. This motivates the division of a cell into further non-overlapping regions, whereby the intercell interference can be avoided having reduced number of users with same sub-bands, and reducing the cell edge effects. In this work, we

alleviate the problem of interference by dividing the macrocells into multiple regions such as 4, 8 and 16, etc, where the users having same sub-carriers can be placed apart, thus, the path loss between them increases, this results in subsequently mitigating the problem of interference [44].

## 3.2 System Model of W-RFA in a multi-cell scenario

We consider the downlink of a heterogeneous cellular network consisting of macrocells, in which the circular-shaped femtocells are uniformly distributed. The entire region of a macrocell is partitioned into $w$ disjoint regions of equal area, where

$w = 2^l$, such that $l \epsilon \mathbb{N}$ and $\mathbb{N}$ is the set of natural numbers, hence $w = \{2, 4, 8, 16\}$, results in 2-RFA, 4-RFA, 8-RFA and 16-RFA, respectively[1]. The allocated frequency spectrum, $B$, is partitioned among $k$ orthogonal sub-bands. Sub-carrier allocation is performed by assuming that the users are uniformly distributed within the multiple regions of a macrocell. We consider the in-band transmission of femtocells, i.e., both pico and macro users utilize the same frequency spectrum. Furthermore, frequency division duplexing (FDD) is considered, where each available sub-band further splits into equal uplink and downlink frequency bands of $x$ and $y$, such that $B_t = [B_{tx} \bigcup B_{ty}]; t = \{1, 2, ....., k\}$.

In this work, we adopt the same strategy of 2-RFA and implemented into

[1]It can be noticed that, theoretically, a higher region RFA is possible. However, we will later show that the sum rate saturates after a particular division. Hence, we focus on smaller value of $l$, i.e., $l = 4$.

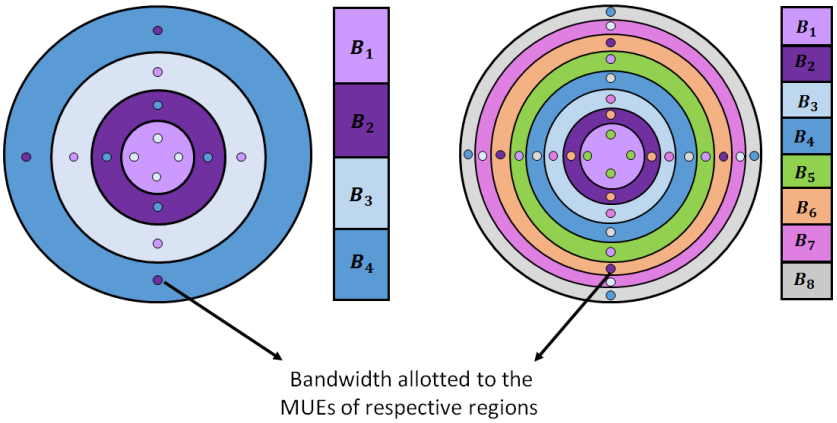


Figure 3.3: Frequency allocation in a single cell (4-RFA and 8-RFA).

higher region RFA. In 4-RFA, the entire spectrum is split into 4 sub-bands $B_1$, $B_2$, $B_3$ and $B_4$, in the respective 4 regions $\{R_1, R_2, R_3, R_4\}$ of equal area as shown in the left side of Fig. 3.3. In $R_1$ region, one of the PBS acts as serving BS for downlink PUE, whereas rest of the PBSs behave as a source of interference, also the MUEs of $R_3$ act as interferers. Likewise, $R_2$ DL PUEs encounter cross-tier interference from $R_4$ MUEs. This is due to increased path loss that provide a negligible interference. Similarly, $R_3$ PUEs receive interference from $R_1$, and $R_4$ PUEs from $R_2$ MUEs. The benefit of dividing macrocells into higher regions is that the number of PUEs and MUEs are now divided among more regions and the reduction of number of picocells in a specific region utilizing the same frequency spectrum is achieved. Hence, the cell edge interference is minimized because none of the same frequency sub-bands is allocated in adjacent cells, which was the case in 2-RFA multi-cell, thus minimizing the overall system outage probability.

In case of 8-RFA, the whole area splits into 8 equal regions and similarly

the frequency spectrum is also divided as shown in the right side of Fig. 3.3. In this way, the interference regions are located farther apart, i.e., now $R_1$ will experience cross-tier interference from $R_5$, $R_2$ from $R_6$, $R_3$ from $R_7$ and $R_4$ from $R_8$, respectively. Hence, the PUEs in every region receive interference from a distant region as compared to their adjacent regions. Moreover, because of reduced area, the number of interfering users also reduces, this results in higher SINR values. On the other hand, as the frequency spectrum is further divided among the regions, we achieve better coverage at the cost of sum capacity reduction. Further reduction in average outage probability can be achieved if we continue dividing the whole area, e.g., in 16-RFA, the interfering regions are now far apart from each other.

Partitioning the macro-cells into further non-overlapping regions of equal area reduces not only the intracell but also the intercell interference. The MUEs and PBSs of neighboring cells utilizing same spectrum, are spaced further apart, thereby decreasing the level of interference. When 4-RFA scheme is extended in multi-cell, the interfering cells experience maximum attenuation in their signals, i.e., the distance between the intended cell and interfering cells is increased, which is evident in Fig. 3.3. It can be observed from the figure that the cell edge PUEs in $R_4$ do not receive any co-tier interference from the adjacent regions of neighboring cells but only cross-tier interference from low powered MUEs from two neighboring cells. Thereby, the impact of interference becomes negligible, as a consequence higher SINR is achieved. By opting the other higher region RFA schemes, for instance, 8-RFA and 16-RFA, the chance that the PUEs receive interference from the adjacent regions of other cells declines further, however, the

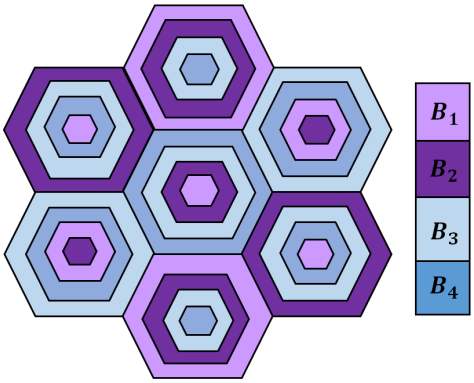


Figure 3.4: 4-RFA in a multi-cell scenario. The cell area is divided into four regions with frequency bands $B_1$, $B_2$, $B_3$ and $B_4$.

issue of availability of smaller sub-bands to the users still persists. On the other hand, implementing the M-4-RFA scheme in multicell, the number of interfering entities in the adjacent regions of other cells is reduced and the remaining users in the alternative regions utilizing same spectrum are spaced apart. In this way, maximum benefit from the bandwidth can be exploited by making the impact of interference negligible. Therefore, M-4-RFA provides significant gains even when cross-tier interference of multi-cell is considered. However, partitioning the cell into higher regions is not a practical solution for interference management as smaller the area of the region, more frequent handover occurs. Similarly, accurate localization systems would be required that become an expensive solution with redundant infrastructure. Therefore, our aim is to find an optimized scheme that divides the cell into higher regions but also generates a notable increase in the data rates. For W region RFA, the generalized expression of SINR of downlink PUEs in multi-cell is expressed as

$$SINR = \frac{P_p h_i ||x_i||^{-\beta_2}}{\Sigma_{c \epsilon C_m} \Sigma_{q=1, q \neq i}^{\Psi} P_p h_q ||x_q||^{-\beta_2} + \Sigma_{c \epsilon C_m} \Sigma_{m=1}^{\Omega} P_m h_m ||x_m||^{-\beta_1} + \sigma^2}, \quad (3.2)$$

where the second summation represents the interference caused by PBSs and MUEs from the neighboring cells and $C_m = \{1, 2, ...., C\}$, is a set that represents the number of neighboring cells. As the users at the edge experience enormous ICI, a power factor ($\lambda$) is introduced to minimize the impact of this interference.

In this way, if an MUE is located in the center region, the transmit power is given by $P_i$, whereas if MUE is in outer region near the edges, the transmit power is $P_o = \lambda P_i$, where $\lambda > 1$.

The average outage probability for a downlink PUE is formulated as

$$\Gamma_{DL} = \mathbb{P}(SINR_{DL\_P} < \delta), \tag{3.3}$$

Therefore, the user that is in coverage must have operating SINR greater than the predefined threshold. The achievable sum rate at downlink PUEs can be calculated using the Shannon-Hartley theorem given as

$$\rho_{DL} = \Delta B log_2(1 + SINR_{DL\_P}), \tag{3.4}$$

where $\Delta B$, is the sub-carrier bandwidth that is allocated to the users in a specific region, $\Delta B = B/N$, where $B$ is the system bandwidth, $N$ is the total number of sub-bands such that $N = 2^M$; $M = \{2, 3, 4, 5\}$ for 2, 4, 8 and 16, RFA respectively.

Table 3.2: Frequency Distribution in Modified 4-RFA Method.

| | | | | | | | |
|---|---|---|---|---|---|---|---|
| $\mathbf{B}_1$ | | | | $\mathbf{B}_2$ | | | |
| $R_1$ Pico UL | $R_1$ Pico DL | $R_3$ Pico UL | $R_3$ Pico DL | $R_2$ Pico UL | $R_2$ Pico DL | $R_4$ Pico UL | $R_4$ Pico DL |
| $B_{1x}$ | $B_{1y}$ | $B_{1x}$ | $B_{1y}$ | $B_{2x}$ | $B_{2y}$ | $B_{2x}$ | $B_{2y}$ |
| $R_2$ Macro DL | $R_2$ Macro UL | $R_4$ Macro DL | $R_4$ Macro UL | $R_1$ Macro DL | $R_1$ Macro UL | $R_3$ Macro DL | $R_3$ Macro UL |

## 3.3 Modified RFA schemes

The focus of this work is to maximize the sum capacity of downlink PUEs. Although the division of macrocells into higher regions minimizes the number of interfering entities, however, it is accompanied by the reduction of channel bandwidth available to each user (MUE and/or PUE), as a consequence overall throughput of the system is decreased. Thus, in spite of simply dividing the regions and bandwidth, we propose to allocate the frequency in an efficient manner that can provide maximum vulnerability to interference, for gaining desired sum rates along with minimum outage. For instance, we can merge the benefits of both 2-RFA & 4-RFA and devise a scheme known as *modified-4-RFA (M-4-RFA)*. In M-4-RFA scheme, the cell is divided into four regions, just as we do in regular 4-RFA, however, each region now gets co-tier interference from two regions (as opposed to single region in 4-RFA). The pico users of region $R_1$ receive co-tier interference from the same region and from $R_3$. Similarly, cross-tier interference from $R_2$ and $R_4$. On the other hand, $R_2$ PUEs experience co-tier interference from $R_2$ and $R_4$, whereas cross-tier interference from $R_1$ and $R_3$ as explained in Table 3.2. The SINR

of DL PUEs for this scheme can be calculated using following expression

$$SINR = \frac{P_p h_i ||x_i||^{-\beta_2}}{\Sigma_{c\epsilon C_m} \Sigma_{u\epsilon R_u} \Sigma_{q=1,q\neq i}^{\Psi} P_p h_q ||x_q||^{-\beta_2} + \Sigma_{c\epsilon C_m} \Sigma_{u\epsilon R_u} \Sigma_{m=1}^{\Omega} P_m h_m ||x_m||^{-\beta_1} + \sigma^2}, \quad (3.5)$$

where $R_u$ represents the number of regions in each neighboring cell, $C_m$, causing interference to the intended PUE. The procedure of calculating the SINR is presented in Algorithm 3.1. Therefore, by adopting this scheme, the impact of interference is little enhanced as compared to regular 4-RFA (because of additional interfering regions), however, the sub-carriers are divided as in 2-RFA, hence elevating the data rates. The MUEs that share the same sub-band have different powers and also they are moved apart, therefore, the influence caused by the interfering cells is reduced. The ICI when compared to regular 2-RFA is also minimized, as the number of interfering cells in the outer regions of the neighboring cells is reduced. Similar concept can be applied to form M-8-RFA by dividing the cell into 8 regions and utilizing the sub-bands of 4-RFA, alternatively in the regions of each cells. M-16-RFA can also be devised by using sub-carriers of lower RFA schemes (4-RFA or 8-RFA). To evaluate the performance of this hybrid scheme, we define outage capacity, which is formulated as

$$\psi_{\_ot\_DL} = (1 - \Gamma_{DL}) \Delta B log_2(1 + SINR_{DL\_P}), \quad (3.6)$$

and is used to capture a complete picture of system by taking end-to-end success as well as rates into consideration.

**Algorithm 3.1** *Interference calculation algorithm for M-RFA.*

***Initialization.***

*A set of P PUEs, where i = {1,....,P}.*

*A set of PB PBSs, where j = {1,....,PB}.*

*A set of M MUEs, where m = {1,....,M}*

***Iteration***

`for each PUE p`

*PUE association with serving PBS is based on highest*

*received signal power strength.*

*Calculate the interference from PBSs and MUEs accordingly.*

***for*** `i = 1 to P` ***do***

***for*** `j = 1 to PB` ***do***

$s_{ij} \leftarrow$ *matrix that contains the interference from all the PBSs of other respective regions*

***if*** *i==j* ***then***

***else***

$e_{ij} \leftarrow$ *matrix that contains the interference from the PBSs of the region from which PUE belongs.*

***end if***

***end for***

***end for***

***for*** `m = 1 to M` ***do***

$U_m \leftarrow$ *matrix that calculates the interference from the respective region MUEs to the considered PUE.*

***end for***

# Chapter 4

# Mathematical Modeling of RFA Scheme

In this chapter, we present analytical expressions for the coverage probabilities of DL PUEs in a heterogeneous two tier cellular network, i.e., pico cells are overlaid with macro cellular network. To calculate the coverage of the networks, it is considered that a conventional hexagonal grid model provides an upper bound on coverage, i.e., the deployment of BSs having deterministic cell boundaries is a widely used approach for simulations but too idealistic for practical scenarios. Therefore, in [45], it is stated that a PPP distribution could be used that helps in the modeling of these networks through stochastic geometry. In such models, the BSs have cell boundaries corresponding to Voronoi tessellations where the BSs locations are modeled by a PPP of finite intensity. Recently, in [47], it is explained that by assuming BS coverage area as Voronoi tessellations, accuracy in the modeling of coverage probability is achieved for higher values of path loss exponent, i.e., 4 or higher, whereas

for smaller values of path loss exponent, e.g., 2.5, the performance of model is not matched accurately.

Therefore, to provide the tractable coverage probability expressions for a vast variety of parameters, we perform the modeling of the network using two approaches; in the first approach, the PBSs are spatially modeled as a PPP, and interference is calculated through Laplace transform whereas in the second approach, the expected value of interference is calculated using the fluid model [48], where the distribution of users and BSs is assumed to be uniformly random and results are valid even for smaller values of path loss exponent.

## 4.1 Coverage probability analysis considering PPP

As mentioned earlier, a closed access mode is considered, i.e., each user is connected to the closest BS of a particular tier [46]. For a 2-RFA scheme, we divide the macro cell into 2 regions of equal area. The distribution of PBSs and MUEs in each region is considered as independent PPPs, $\Phi_j^{(\nu)}$ of intensity $\lambda_j^{(\nu)}$ and $\Phi_k^{(\nu)}$ of intensity $\lambda_k^{(\nu)}$, respectively, where $\nu$ denotes the regions of macrocell, i.e, $\nu \in \{1, 2\}$ for 2-RFA. Each user is served by at most one pico BS with transmit power $P_p$ and the user can communicate with the tagged BS if the resulting SINR is greater than a pre-defined threshold $\tau$. Without loss of generality, it is assumed that the user is at the origin. Hence, the received power at the user from a PBS located at distance $x_i^{(1)}$

is given as $P_p h_i^{(1)} ||x_i^{(1)}||^{-\beta_2}$. As far as interference is concerned, a worst case scenario is assumed in which all the PBSs and MUEs that utilize the same spectrum are transmitting, therefore a user experiences interference from all the interfering entities. The generalized expression of SINR for a downlink pico user located in the inner region $R_1$ of macro cell connected to its PBS of same region is expressed as

$$SINR_x^{(1)} = \frac{P_p h_i^{(1)} ||x_i{}^{(1)}||^{-\beta_2}}{I_{pbs} + I_{mue} + \sigma^2}\,, \tag{4.1}$$

where $I_{pbs}$ is the interference from the downlink PBSs located in $R_1$ and $I_{mue}$ represents the interference active form all the transmitting uplink MUEs from region $R_2$, respectively, both are expressed in the following expressions

$$I_{pbs} = \sum_{\substack{x_j^{(1)} \in \Phi_j^{(1)} \\ x_j^{(1)} \neq x_i^{(1)}}} P_p h_j^{(1)} ||x_j^{(1)}||^{-\beta_2},$$

$$I_{mue} = \sum_{x_k^{(2)} \in \Phi_k^{(2)}} P_m h_k^{(2)} ||x_k^{(2)}||^{-\beta_1},$$

### 4.1.1 Distance to the closest Pico base station

Since, each user connects with the closest base station, no other base station can be closer than $x_i^{(1)}$, in other words all the other PBSs are at least at the distance $\chi$ from the user. For the sake of simplicity, we drop the subscript $i$ and represent the distance between the serving PBS and user as $x^{(1)}$. Then probability density function (PDF) of $x^{(1)}$ can be formulated by utilizing the

fact that the null probability of Poisson point in an area is $\exp(\lambda a)$.

$$\mathbb{P}[x^{(1)} > \chi] = e^{-\lambda_j^{(1)}\pi\chi^2}.$$

Therefore, the cumulative distribution function (CDF) is

$$\mathbb{P}[x^{(1)} \leq \chi] = 1 - e^{-\lambda_j^{(1)}\pi\chi^2},$$

The PDF then becomes

$$f(x^{(1)}) = \frac{dF(x^{(1)})}{dx^{(1)}} = 2\pi\lambda_j^{(1)} x^{(1)} e^{-\pi\lambda_j^{(1)} {x^{(1)}}^2}.$$

### 4.1.2 Coverage Probability

Given the SINR threshold and path loss exponent, the coverage probability is expressed as

$$P_c^{(1)}(\tau) = \int_{x^{(1)}>0} \mathbb{E}_{I_x^{(1)}} \left[\mathbb{P}[SINR_x^{(1)} > \tau]\right] f(x^{(1)}) dx^{(1)}, \tag{4.2}$$

$$\begin{aligned} &= \int_{x^{(1)}>0} \mathbb{E}_{I_x^{(1)}} \left[\mathbb{P}\left(h > \tau (P_p)^{-1} {x^{(1)}}^{\beta_2} (I_x^{(1)} + \sigma^2)\right)\right] \\ &2\pi\lambda_j^{(1)} x^{(1)} e^{-\pi\lambda_j^{(1)} {x^{(1)}}^2} dx^{(1)} \end{aligned} \tag{4.3}$$

The probability that the SINR is greater than $\tau$ is

$$\begin{aligned} &\mathbb{E}\left[\mathbb{P}\left(h > \tau (P_p)^{-1} {x^{(1)}}^{\beta_2} (I_{pbs} + I_{mue} + \sigma^2)\right)\right] \\ &= exp\left(\frac{-\tau\sigma^2}{P_p {x^{(1)}}^{-\beta_2}}\right) \mathbb{E}\left(e^{\frac{-\tau(I_{pbs}+I_{mue})}{P_p {x^{(1)}}^{-\beta_2}}}\right), \end{aligned} \tag{4.4}$$

By putting the value of expectation obtained in (5) back into (4), it can be further simplified as

$$= 2\pi\lambda_j^{(1)} \int_{\mathbb{R}^2} \mathcal{L}_{I_{pbs}}(s)\, \mathcal{L}_{I_{mue}}(s)\, e^{\frac{-\tau\sigma^2}{P_p x^{(1)-\beta_2}}} e^{-\pi\lambda_j^{(1)} x^{(1)^2}} x^{(1)} dx^{(1)} \tag{4.5}$$

where $\mathcal{L}_{I_{pbs}}(.)$ and $\mathcal{L}_{I_{mue}}(.)$ are the Laplace transform of interference from the DL PBSs and UL MUEs from the respective regions and are given in the following Lemmas,

**Lemma 1:**

$$\mathcal{L}_{I_{pbs}}(s) = exp\Big(-\pi x^{(1)^2} \lambda_j^{(1)} \tau^{2/\beta_2} C_2^{(1)}\Big), \tag{4.6}$$

*Proof:*

The Laplace transform definition yields

$$\mathcal{L}_{I_{pbs}}(s) = \mathbb{E}\left[e^{-sI_{pbs}}\right],$$

$$= \mathbb{E}\left[exp\left(-s \sum_{x_j^{(1)} \in \Phi_j^{(1)}/x^{(1)}} P_p h_j^{(1)} ||x_j^{(1)}||^{-\beta_2}\right)\right], \tag{4.7}$$

$$= \mathbb{E}\left[\prod_{x_j^{(1)} \in \Phi_j^{(1)}/x^{(1)}} exp\left(-sP_p h_j^{(1)} ||x_j^{(1)}||^{-\beta_2}\right)\right], \tag{4.8}$$

$$= \mathbb{E}_{\Phi_j^{(1)}}\left[\prod_{x_j^{(1)} \in \Phi_j^1/x^{(1)}} \frac{1}{1 + sP_p ||x_j^{(1)}||^{-\beta_2}}\right], \tag{4.9}$$

The channel gains are Rayleigh fading and are independent of PPP, the sum over PPP leads to the product form in (4.8) and the moment generating function of an exponential random variable yields (4.9), finally applying the

probability generation functional (PGFL) of PPP we obtain (4.10). Transformation of Cartesian to polar coordinates $x_j^{(1)} = (r, \theta)$, the final expression of Laplace transform is obtained.

$$= exp\left(\lambda_j^{(1)} \int_{\mathbb{R}^2/x^{(1)}} (1 - \frac{1}{1 + sP_p||x^{(1)}||^{-\beta_2}})dx^{(1)}\right), \tag{4.10}$$

$$= exp\left(-2\pi\lambda_j^{(1)} \int_{x^{(1)}}^{R_1} (1 - \frac{1}{1 + sP_p r^{-\beta_2}})rdr\right), \tag{4.11}$$

where $R_1$ is the radius of region 1 of macrocell, thus the interference is calculated from all the PBSs present in this region other the serving BS at distance $x^{(1)}$, by implementing the change of variables $u^{(1)} = \tau^{-2/\beta_2}(\frac{r}{x^{(1)}})^2$, the Laplace transforms can be further simplified as

$$\mathcal{L}_{I_{pbs}}(s) = exp\Big( - \pi {x^{(1)}}^2 \lambda_j^{(1)} \tau^{2/\beta_2} C_2^{(1)}\Big) \tag{4.12}$$

where $C_2^{(1)} = \int_{\tau^{-(2/\beta_2)}}^{\tau^{-(2/\beta_2)}(R_1/x^{(1)})^2} (\frac{1}{1+(u^{(1)\beta_2/2})})du^{(1)}$

**Lemma 2:**

$$\mathcal{L}_{I_{mue}}(s) = exp\Big(-\pi {x^{(1)}}^2 \lambda_k^{(2)} \tau^{2/\beta_1} C_1^{(2)}\Big), \tag{4.13}$$

*Proof:*

The Laplace transform of cumulative interference from the MUEs located in $R_2$ is given as

$$\mathcal{L}_{I_{mue}^{(2)}}(s) = \mathbb{E}\left[e^{-sI_{mue}}\right],$$

$$= \mathbb{E}\left[exp\left(-s\sum_{x_k^{(2)}\in\Phi_k^{(2)}} P_m h_k^{(2)}||{x_k}^{(2)}||^{-\beta_1}\right)\right], \tag{4.14}$$

$$= \mathbb{E}\left[\prod_{x_k^{(2)}\in\Phi_k^{(2)}} exp\left(-sP_m h_k^{(2)}||{x_k}^{(2)}||^{-\beta_1}\right)\right], \tag{4.15}$$

$$= \mathbb{E}_{\Phi_k^2}\left[\prod_{x_k^{(2)}\in\Phi_k^2} \frac{1}{1+sP_m||{x_k}^{(2)}||^{-\beta_1}}\right], \tag{4.16}$$

$$= exp\left(\lambda_k^{(2)}\int_{\mathbb{R}^2}(1-\frac{1}{1+sP_m||x^{(2)}||^{-\beta_1}})dx^{(2)}\right), \tag{4.17}$$

$$= exp\left(-2\pi\lambda_k^{(2)}\int_{R_1}^{R_2}(1-\frac{1}{1+sP_m r^{-\beta_1}})rdr\right), \tag{4.18}$$

where $R_1$ and $R_2$ defines the boundary of the annular region of macrocell, by following the same procedure as in Lemma 2 and implementing the change of variable $w^{(2)} = (\frac{\tau P_m}{P_p}x^{(1)\beta_2})^{-2/\beta_1}(r)^2$, the Laplace transforms can be further simplified as

$$\mathcal{L}_{I_{mue}}(s) = exp\left(-\pi {x^{(1)}}^2\lambda_k^{(2)}(\frac{\tau P_m}{P_p})^{2/\beta_1}C_1^{(2)}\right), \tag{4.19}$$

where $C_1^{(2)} = \int_{(\frac{\tau P_m}{P_p x^{(1)-\beta_2}})^{-2/\beta_1}(R_1)^2}^{(\frac{\tau P_m}{P_p x^{(1)-\beta_2}})^{-2/\beta_1}(R_2)^2}(\frac{1}{1+(w^{(2)\beta_1/2})})dw^{(2)}$

**Theorem 1:** The probability of coverage of a randomly located DL PUE in $R_1$ can be computed as

$$P_c^{(1)}(\tau) = \pi\lambda_j^{(1)} \int_0^{\infty} exp\Big( - \pi v^{(1)}\lambda_j^{(1)} - \pi v^{(1)}\lambda_j^{(1)}\tau^{2/\beta_2} C_2^{(1)} \\ - \pi v^{(1)}\lambda_k^{(2)} \left(\frac{\tau P_m}{P_p}\right)^{2/\beta_1} C_1^{(2)} - (\frac{\tau\sigma^2}{P_p} v^{(1)^{\beta_2/2}})\Big) dv^{(1)}, \tag{4.20}$$

where $C_2^{(1)} = \int_{\tau^{-(2/\beta_2)}}^{\tau^{-(2/\beta_2)}(R_1/x^{(1)})^2} (\frac{1}{1+(u^{(1)^{\beta_2/2}})}) du^{(1)}$ and

$$C_1^{(2)} = \int_{(\frac{\tau P_m}{P_p x^{(1)^{-\beta_2}}})^{-2/\beta_1}(R_1)^2}^{(\frac{\tau P_m}{P_p x^{(1)^{-\beta_2}}})^{-2/\beta_1}(R_2)^2} (\frac{1}{1+(w^{(2)^{\beta_1/2}})}) dw^{(2)}$$

*Proof:* The final expression for the coverage probability is obtained by plugging the values of Laplace transforms of interferences form the DL PBSs (4.6) and from UL MUEs (4.13) into (4.5) and simplifying, with a final substitution of $v^{(1)} = x^{(1)^2}$. Following the same procedure, the coverage probability of DL PUE located in $R_2$ can be derived and the final expression is given as

$$P_c^{(2)}(\tau) = \pi\lambda_j^{(2)} \int_0^{\infty} exp\Big( - \pi v^{(2)}\lambda_j^{(2)} - \pi v^{(2)}\lambda_j^{(2)}\tau^{2/\beta_2} C_2^{(2)} \\ - \pi v^{(2)}\lambda_k^{(1)} \left(\frac{\tau P_m}{P_p}\right)^{-2/\beta_1} C_1^{(1)} - (\frac{\tau\sigma^2}{P_p} v^{(2)^{\beta_2/2}})) dv^{(2)}, \tag{4.21}$$

where $C_2^{(2)} = \int_{\tau^{-(2/\beta_2)}(R_1/x^{(2)})^2}^{\tau^{-(2/\beta_2)}(R_2/x^{(2)})^2} (\frac{1}{1+(u^{(2)^{\beta_2/2}})}) du^{(2)}$ and

$$C_1^{(1)} = \int_{(\frac{\tau P_m}{P_p x^{(2)^{-\beta_2}}})^{-2/\beta_1}(x^{(1)})^2}^{(\frac{\tau P_m}{P_p x^{(2)^{\beta_2}}})^{-2/\beta_1}(R_1)^2} (\frac{1}{1+(w^{(1)^{\beta_1/2}})}) dw^{(1)}.$$

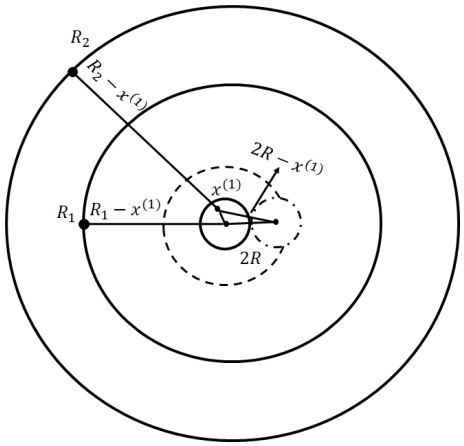


Figure 4.1: Integration limits for cumulative interference computation.

## 4.2 Coverage probability analysis using fluid model

The coverage probability modeling for smaller path loss exponent values can be performed using the fluid model [48]. In this approach, we approximate the average value of interference, by replacing the interfering entities by an equivalent continuum of transmitters, assuming that the PBSs and MUEs are uniformly distributed in the network. Hence, network can be characterize by the PUE density $\rho_{PUE}^{(\nu)}$, PBSs density $\rho_j^{(\nu)}$, and MUE density $\rho_k^{(\nu)}$, respectively. The basic concept of this approach is illustrated in Fig. 4.1, where the network boundary is assumed to be circular having a radius $R_2$, i.e, outer region of 2-RFA. The serving PBS is located at the origin, having a circular coverage area of radius $R$. The PUE is situated at a distance $x^{(1)}$ within the coverage area of that PBS. The cumulative interference from both tiers is calculated by dividing the network into rings as explained in the following section.

### 4.2.1 Approximate cumulative interference calculation

The interference from the PBSs having density $\rho_j^{(1)}$ to the intended PUE in the elementary surface $rdrd\theta$ is given as $\rho_j^{(1)} rdrd\theta$, whereas from MUEs having density $\rho_k^{(2)}$ to the PUE is depicted as $\rho_k^{(2)} rdrd\theta$. Hence, the contribution of co-tier as well as cross-tier interference is $P_p h_j^{(1)} r^{-\beta_2} \rho_j^{(1)} rdrd\theta$ and $P_m h_k^{(2)} r^{-\beta_1} \rho_k^{(2)} rdrd\theta$, respectively. From the Fig. 4.1, it is evident that the distance between the two neighboring PBSs is $2R$, where coverage radius $R \propto \sqrt{\mathbb{E}[Area]}$. Therefore, the distance between the PUE to the closest interfering PBS is taken as $2R - x^{(1)}$. Extending the same concept, the integration surface for the PBSs is approximated with a ring having an inner radius $2R - x^{(1)}$ and outer radius $R_1 - x^{(1)}$. In the similar way, the interference from MUEs is approximated from $R_1 - x^{(1)}$ to $R_2 - x^{(1)}$. Thus, the interference expression can be given as

$$\begin{aligned} I(x^{(1)}) &= \int_0^{2\pi} \int_{2R-x^{(1)}}^{R_1-x^{(1)}} \rho_j^{(1)} P_p h_j^{(1)} r^{-\beta_2} rdrd\theta \\ &+ \int_0^{2\pi} \int_{R_1-x^{(1)}}^{R_2-x^{(1)}} \rho_k^{(2)} P_m h_k^{(2)} r^{-\beta_1} rdrd\theta, \end{aligned} \tag{4.22}$$

$$\begin{aligned} &= \frac{2\pi\rho_j^{(1)} P_p h_j^{(1)}}{\beta_2 - 2} \left[ (2R - x^{(1)})^{(2-\beta_2)} - (R_1 - x^{(1)})^{(2-\beta_2)} \right] \\ &+ \frac{2\pi\rho_k^{(2)} P_m h_k^{(2)}}{\beta_1 - 2} \left[ (R_1 - x^{(1)})^{(2-\beta_1)} - (R_2 - x^{(1)})^{(2-\beta_1)} \right], \end{aligned} \tag{4.23}$$

where $R$ is the radius of serving PBS, $R_1$ and $R_2$ are the radius of inner and outer region of macrocell. Eventually, the average value of the cumulative

interference can be computed as

$$\begin{aligned}\mathbb{E}_{I_x^{(1)}} &= \frac{2\pi\rho_j^{(1)}P_p}{\beta_2-2}\left[(2R-x^{(1)})^{(2-\beta_2)}-(R_1-x^{(1)})^{(2-\beta_2)}\right] \\ &+ \frac{2\pi\rho_k^{(2)}P_m}{\beta_1-2}\left[(R_1-x^{(1)})^{(2-\beta_1)}-(R_2-x^{(1)})^{(2-\beta_1)}\right].\end{aligned} \tag{4.24}$$

### 4.2.2 Coverage probability

The expression for the coverage probability is achieved by assuming the uniform distribution of interferers, distributed over the circular regions of equal area, the resulting CDF is

$$\mathbb{P}[x^{(1)} \leq \chi] = \frac{\chi^2}{df^2}\rho, \qquad 0 \leq \chi \leq R$$

where $\rho$ represents the combined density of the interfering entities in both the regions, $df^2$ is the empirically calculated value act as normalizing factor. The value of this factor depends upon the shape of the coverage area of BS we are assuming [47]. Thus, the PDF is expressed as

$$f(x^{(1)}) = \frac{2x^{(1)}}{df^2}\rho, \qquad 0 \leq x^{(1)} \leq R.$$

Theorem 2: (Approximate Coverage probability using fluid model) The lower bound for the coverage probability $P_c(\tau)$ of randomly chosen DL subscriber connected to PBS located in $R_1$ is given as

$$P_c^{(1)}(\tau) = \frac{\rho}{df^2}\int_0^{R^2} exp\left(-\tau v^{(1)\beta_2/2}\gamma^{(1)}(\beta, v^{(1)})\right) dv^{(1)}, \tag{4.25}$$

*Proof:*

$$P_c^{(1)}(\tau) = \mathbb{E}_x^{(1)}\left[\mathbb{E}_{I_x^{(1)}}\,\mathbb{P}\left(SINR_x^{(1)} > \tau\right)\right], \tag{4.26}$$

$$P_c^{(1)}(\tau) = \frac{\rho}{df^2}\int_0^R \mathbb{E}_{I_x^{(1)}}\left[\mathbb{P}\left(h > \tau P_p^{-1}x^{(1)^{\beta_2}}(\sigma^2 + I_x^{(1)})\right)\right] 2x^{(1)}dx^{(1)} \tag{4.27}$$

Expected value of inner probability can be further simplified as

$$\mathbb{E}_{I_x^{(1)}}\left[\mathbb{P}[h > \tau P_p^{-1}x^{(1)^{\beta_2}}(\sigma^2 + I_{pbs} + I_{mue})]\right]$$

$$= \mathrm{e}^{(-\tau P_p^{-1}x^{(1)^{\beta_2}}\sigma^2)}\mathbb{E}_{Ix}^{(1)}\left[exp(-P_p^{-1}\tau x^{(1)^{\beta_2}}(I_{pbs} + I_{mue}))\right], \tag{4.28}$$

According to Jensen's inequality we have

$$\mathbb{E}_{I_x^{(1)}}\left[exp\left(-\tau P_p^{-1}x^{(1)^{\beta_2}}I_x^{(1)}\right)\right] \geq exp\left(-\tau P_p^{-1}x^{(1)^{\beta_2}}\mathbb{E}_{I_x^{(1)}}\right), \tag{4.29}$$

By substituting the expected value of interference obtained from (13) in (18) we get

$$\mathbb{E}_{I_x^{(1)}}\left[exp(-\tau P_p^{-1}x^{(1)^{\beta_2}}I_x\right] \geq exp(-\tau x^{(1)^{\beta_2}}\gamma^{(1)}(\beta, v^{(1)}), \tag{4.30}$$

where

$$\gamma^{(1)}(\beta, v^{(1)}) = \frac{\sigma^2}{P_p} + \frac{2\pi\rho_j^{(1)}}{\beta_2 - 2}\alpha^{(1)} + \frac{2\pi\rho_k^{(2)}P_m}{P_p(\beta_1 - 2)}\mu^{(2)},$$

where $\alpha^{(1)} = [(2R - {v^{(1)}}^{1/2})^{(2-\beta_2)} - (R_1 - {v^{(1)}}^{1/2})^{(2-\beta_2)}]$ and $\mu^{(2)} = [(R_1 - {v^{(1)}}^{1/2})^{(2-\beta_1)}$

-$(\mathrm{R}_2 - {v^{(1)}}^{1/2})^{(2-\beta_1)}]$, substituting ${x^{(1)}}^2 = v^{(1)}$ in the above equation and putting the value in (4.27), we get the final expression of coverage probability with interferers having uniformly distribution over the respective regions and

this completes the proof.

Following the similar procedure the coverage probability of users located in $R_2$ can be derived. The final expressions is given as

$$P_c^{(2)}(\tau) = \frac{\rho}{df^2} \int_0^{R^2} exp\left(-\tau {v^{(2)}}^{\beta/2} \gamma^{(2)}(\beta_2, v^{(2)})\right) dv^{(2)}, \tag{4.31}$$

where

$$\gamma^{(2)}(\beta, v^2) = \frac{\sigma^2}{P_p} + \frac{2\pi\rho_1 P_m}{P_p(\beta_1 - 2)}\alpha^{(2)} + \frac{2\pi\rho_2}{\beta_2 - 2}\mu^{(1)}, \tag{4.32}$$

where $\alpha^{(2)} = [(2R - {v^{(2)}}^{1/2})^{(2-\beta_1)} - (2R + R_1 - {v^{(2)}}^{1/2})^{(2-\beta_1)}]$,

and $\mu^{(1)} = [(R_1 - {v^{(2)}}^{1/2})^{(2-\beta_2)} - (2R + R_2 - {v^{(2)}}^{1/2})^{(2-\beta_2)}]$, respectively.

**Remarks:** Now that we have derived the analytical coverage probability expressions for the 2-RFA, the similar procedure is followed for the higher region RFA schemes. As DL PUEs in any region receive co-tier as well as cross-tier interference only from one region. Therefore, the aforementioned analysis cab be extended easily. In the subsequent section, we provide the expressions for M-4-RFA and explain the modification that occurs in the network while implementing this scheme.

## 4.3 Coverage probability analysis of M-4-RFA:

Division of a macrocell reduces the number of interfering entities that utilize the same spectrum, thus minimizes the outage, in addition also alleviates the throughput of the DL PUEs. Therefore, we opt for a moderate option

in which we divide the macrocell into 4 regions, however, in this scheme a litter higher interference is achieved as compared to the corresponding 4 region RFA scheme but the users are provided with the higher rates due to enhanced SINR values as the interferers are move in the far apart regions. The SINR expression for a DL PUE located in $R_1$ in modified 4-RFA is given as

$$SINR_x^{(1)} = \frac{P_p h_i^{(1)} ||x_i{}^{(1)}||^{-\beta_2}}{I_{pbs} + I_{mue} + \sigma^2}, \tag{4.33}$$

where $I_{pbs}$ is the interference from the downlink PBSs located in $R_1$ and $R_3$, and $I_{mue}$ represents the interference arriving form all the transmitting uplink MUEs from region $R_2$ and $R_4$, respectively, both are expressed in the following expressions

$$I_{pbs} = \sum_{\substack{x_j^{(1)} \epsilon \Phi_j^{(1)} \\ x_j^{(1)} \neq x_i^{(1)}}} P_p h_j^{(1)} ||x_j^{(1)}||^{-\beta_2} + \sum_{x_l^{(3)} \epsilon \Phi_l^{(3)}} P_p h_l^{(3)} ||x_l^{(3)}||^{-\beta_2},$$

$$I_{mue} = \sum_{x_k^{(2)} \epsilon \Phi_k^{(2)}} P_m h_k^{(2)} ||x_k^{(2)}||^{-\beta_1} + \sum_{x_n^{(4)} \epsilon \Phi_n^{(4)}} P_m h_n^{(4)} ||x_n^{(4)}||^{-\beta_1},$$

where $\Phi_j^{(1)}$ and $\Phi_l^{(3)}$ represent the independent PPPs of PBSs in $R_1$ and $R_3$, and $\Phi_k^{(2)}$, $\Phi_n^{(4)}$ are that of UL MUEs in $R_2$ and $R_4$.

### 4.3.1 Coverage probability using PPP

The analytical expression for the coverage probability can be derived using the similar procedure as above, however, for the interference calculation the Laplace transform now include additional terms. The final expression of PUE

located in $R_1$ can be expressed as

$$P_c^{(1)}(\tau) = \pi\lambda_j^{(1)} \int_0^{\infty} exp\Big( - \pi v^{(1)}\lambda_j^{(1)} - \pi v^{(1)}\lambda_j^{(1)}\tau^{2/\beta_2} C_2^{(1)} - \pi v^{(1)}\lambda_k^{(2)}\tau^{2/\beta_1} C_1^{(2)} \\ \text{-}\pi v^{(1)}\lambda_l^{(3)}\tau^{2/\beta_2} C_2^{(3)} - \pi v^{(1)}\lambda_n^{(4)}\tau^{2/\beta_1} C_1^{(4)} - (\tfrac{\tau\sigma^2}{P_p} v^{(1)^{\beta_2/2}})\Big) dv^{(1)} \tag{4.34}$$

where $C_2^{(1)} = \int_{\tau^{-(2/\beta_2)}}^{\tau^{-(2/\beta_2)}(R_1/x^{(1)})^2} (\frac{1}{1+(u^{(1)^{\beta_2/2}})}) du^{(2)}$,

$$C_2^{(3)} = \int_{\tau^{-(2/\beta_2)}(R_2/x^{(1)})^2}^{\tau^{-(2/\beta_2)}(R_3/x^{(1)})^2} (\frac{1}{1+(u^{(3)^{\beta_2/2}})}) du^{(3)},$$

$$C_1^{(2)} = \int_{\left(\frac{\tau P_m x^{(1)^{\beta_2}}}{P_p}\right)^{-2/\beta_1}(R_1)^2}^{\left(\frac{\tau P_m x^{(1)^{\beta_2}}}{P_p}\right)^{-2/\beta_1}(R_2)^2} (\frac{1}{1+(w^{(2)^{\beta_1/2}})}) dw^{(2)}, \text{ and}$$

$$C_1^{(4)} = \int_{\left(\frac{\tau P_m x^{(1)^{\beta_2}}}{P_p}\right)^{-2/\beta_1}(R_3)^2}^{\left(\frac{\tau P_m x^{(1)^{\beta_2}}}{P_p}\right)^{-2/\beta_1}(R_4)^2} (\frac{1}{1+(w^{(4)^{\beta_1/2}})}) dw^{(4)},$$ whereas the coverage probability expressions for the pico user located in $R_2$, $R_3$, and $R_4$ regions are given as follows.

The impact of cumulative co-tier as well as cross-tier interference from all the four regions is obtained by deriving the Laplace Transform of interference from the DL and UL transmitters, and by following the above mentioned procedure the coverage probability of PUEs located in $R_2$ is given as

$$P_c^{(2)}(\tau) = \pi\lambda_j^{(2)} \int_0^{\infty} exp\Big( - \pi v^{(2)}\lambda_j^{(2)} - \pi v^{(2)}\lambda_j^{(2)}\tau^{2/\beta_2} C_2^{(2)} \\ - \pi v^{(2)}\lambda_k^{(1)}\tau^{2/\beta_1} C_1^{(1)} - \pi v^{(2)}\lambda_l^{(4)}\tau^{2/\beta_2} C_2^{(4)} \\ - \pi v^{(2)}\lambda_n^{(3)}\tau^{2/\beta_1} C_1^{(3)} - (\frac{\tau\sigma^2}{P_p} v^{(2)^{\beta_2/2}})\Big) dv^{(2)}, \tag{4.35}$$

When the PUE is in $R_3$ region, it receives cross-tier interference from $R_2$ and

$R_4$, thus the coverage probability expression becomes

$$P_c^{(3)}(\tau) = \pi\lambda_j^{(3)} \int_0^{\infty} exp\Big( - \pi v^{(3)}\lambda_j^{(3)} - \pi v^{(3)}\lambda_j^{(3)}\tau^{2/\beta_2}C_2^{(3)} - \pi v^{(3)}\lambda_k^{(2)}\tau^{2/\beta_1}C_1^{(2)} - \pi v^{(3)}\lambda_l^{(1)}\tau^{2/\beta_2}C_2^{(1)} - \pi v^{(3)}\lambda_n^{(4)}\tau^{2/\beta_1}C_1^{(4)} - (\frac{\tau\sigma^2}{P_p}v^{(3)^{\beta_2/2}})\Big)dv^{(3)}, \tag{4.36}$$

Finally, the PUE is in $R_4$ region receives cross-tier interference from $R_1$ and $R_3$ and the coverage probability can be expressed as

$$P_c^{(4)}(\tau) = \pi\lambda_j^{(4)} \int_0^{\infty} exp\Big( - \pi v^{(4)}\lambda_j^{(4)} - \pi v^{(4)}\lambda_j^{(4)}\tau^{2/\beta_2}C_2^{(4)} - \pi v^{(4)}\lambda_k^{(3)}\tau^{2/\beta_1}C_1^{(1)} - \pi v^{(4)}\lambda_l^{(2)}\tau^{2/\beta_2}C_2^{(2)} - \pi v^{(4)}\lambda_n^{(1)}\tau^{2/\beta_1}C_1^{(3)} - (\frac{\tau\sigma^2}{P_p}v^{(4)^{\beta_2/2}})\Big)dv^{(4)}, \tag{4.37}$$

**Coverage probability using Fluid model**

The PBSs and MUEs are uniformly distributed in the four regions of the macrocell. Each PUE in any region receive cross-tier as well as co-tier interference from two regions, thus the PUE has to face interference from the four regions. Consequently, following coverage probability expression is obtained

$$P_c^{(1)}(\tau) = \frac{\rho}{df^2} \int_0^{R^2} exp(-\tau v^{(1)\beta_2/2}\psi^{(1)}(\beta, v^{(1)})dv^{(1)}, \tag{4.38}$$

where

$$\psi^{(1)}(\beta, v^{(1)}) = \frac{\sigma^2}{P_p} + \frac{2\pi\rho_j^{(1)}}{\beta_2 - 2}\left[(2R - {v^{(1)}}^{1/2})^{(2-\beta_2)} - (R1 - {v^{(1)}}^{1/2})^{(2-\beta_2)}\right] + \frac{2\pi\rho_k^{(2)}P_m}{P_p(\beta_1 - 2)}\left[(R_1 - {v^{(1)}}^{1/2})^{(2-\beta_1)} - (R_2 - {v^{(1)}}^{1/2})^{(2-\beta_1)}\right] + \frac{2\pi\rho_l^{(3)}}{\beta_2 - 2}\left[(R_2 - {v^{(1)}}^{1/2})^{(2-\beta_2)} - (R_3 - {v^{(1)}}^{1/2})^{(2-\beta_2)}\right] + \frac{2\pi\rho_n^{(4)}P_m}{P_p(\beta_1 - 2)}\left[(R_3 - {v^{(1)}}^{1/2})^{(2-\beta_1)} - (R_4 - {v^{(1)}}^{1/2})^{(2-\beta_1)}\right], \tag{4.39}$$

Following the similar procedure the coverage probability of users located in $R_2$, $R_3$, and $R_4$ can be derived. The final expressions are given as When the pico user is located in $R_2$ region the uniformly distributed PBSs other than the serving PBS in that region act as interferers, along with the PBSs in $R_4$ region, thus by evaluating the expected value of interference as in (25), keeping the fact that now the PUE is located in $R_2$ region, the coverage probability is given as

$$P_c^{(2)}(\tau) = \frac{\rho}{df^2}\int_0^{R^2} exp\left(-\tau {v^{(2)}}^{\beta_2/2}\psi^{(2)}(\beta, v^{(2)})\right) dv^{(2)}, \tag{4.40}$$

Now, when the user is in $R_3$, considering the densities of PBSs and MUEs, the lower bound of coverage probability becomes

$$P_c^{(3)}(\tau) = \frac{\rho}{df^2}\int_0^{R^2} exp\left(-\tau {v^{(3)}}^{\beta_2/2}\psi^{(3)}(\beta, v^{(3)})\right) dv^{(3)}, \tag{4.41}$$

Finally, PUE located in $R_4$, having SINR greater than the given threshold

its coverage is expressed as

$$P_c^{(4)}(\tau) = \frac{\rho}{df^2} \int_0^{R^2} exp\left(-\tau v^{(4)^{\beta_2/2}} \psi^{(4)}(\beta, v^{(4)})\right) dv^{(4)}, \tag{4.42}$$

where $\psi^{(2)}(\beta, v^{(2)})$, $\psi^{(3)}(\beta, v^{(3)})$ and $\psi^{(4)}(\beta, v^{(4)})$, can be obtained by computing the integration limits for cumulative interference similar to (4.15) and (4.39).

## 4.4 Coverage rate analysis

Generally the performance of network is evaluated in terms of eminent coverage improvement and enhanced data rates. In the above sections, the analytical closed-form expressions for the coverage probability have been derived, for the users having SINR greater than some threshold. In this section, exact rate distribution expression termed as rate coverage probability is provided, by the virtue of which the probability that the rate of an intended user is greater than the given threshold can be calculated. The expression for the rate coverage is derived in the following lemma.

**Lemma 3:** Given the SINR coverage probability greater than the threshold $\tau$, $P_c(\tau)$, the coverage rate probability is evaluated as $\mathrm{P}(\delta) = P_c(2^{\delta/\Delta B} - 1)$.

*Proof:* The proof is similar to [49], for $\delta < \Delta B log_2(1+\tau_{max})$, where $\delta$ is the rate threshold, $\Delta B = B/N$, B represents the total system bandwidth and N depicts the number of sub-bands provided to the users of each RFA scheme, like 2, 4, M-4, and 8-RFA scheme. The final expression directly follows

and can be evaluated through a change of variables $P(\delta) = \mathbb{P}[SINR > 2^{\delta/\Delta B} - 1] = P_c(2^{\delta/\Delta B} - 1)$.

# Chapter 5

# RESULTS & SYSTEM PERFORMANCE

In this chapter, we first present the guidelines of proposed multiple region RFA scheme to design the system and evaluate its performance, then the accuracy of analytical expressions for the coverage probability and rate coverage these expressions is validated by simulations.

## 5.1 System performance for multi-cellular network

The simulation environment comprises of two tiers, multicell network comprises of 7 hexagonal macrocells in which the circular shaped picocells are randomly distributed. We assumed closed subscriber group (CSG), in which the MUEs are not allowed to access the services of the respective PBSs. For simplicity, it is assumed that one PUE is associated to each PBS. The path

Table 5.1: Simulation Parameters.

| Parameters | Values |
|---|---|
| System Bandwidth | 10 MHz |
| Macrocell radius | 1 km |
| No. of PBSs | 120 |
| No. of MUEs | 120 |
| Thermal noise | -174 dBm/Hz |
| PBS power | 23 dBm |
| Max. MUE power | 23 dBm |

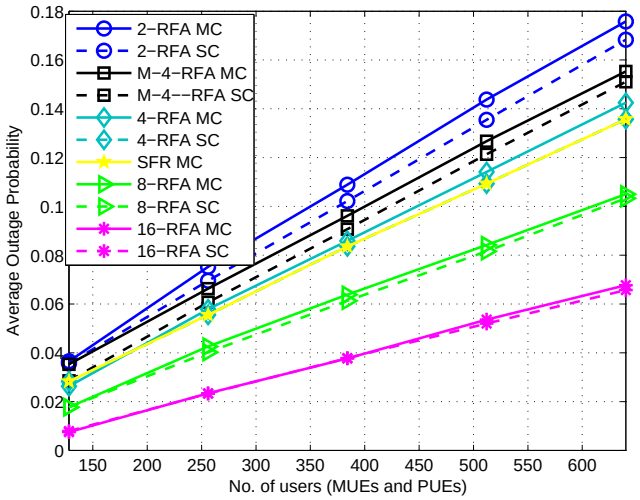


Figure 5.1: Average outage probability of various RFA schemes in single and multi-cell scenarios ( $\tau = 0.4$, $\beta_1 = 3$, $\beta_2 = 2.5$).

loss exponent, $\beta_1$ and $\beta_2$, for MUE and PUE is taken as 3 and 2.5, respectively. The density of MUEs is supposed to be three times greater than that of PUEs is each region. Unless otherwise mentioned, we assume the simulation parameters that are listed in Table 5.1.

Fig. 5.1 represents the average outage probability of 2-RFA, 4-RFA, M-4-RFA, 8-RFA,16-RFA and SFR, in single cell (SC) and multi-cell (MC) scenarios. The figure shows the effects of cell-edge interference and validates

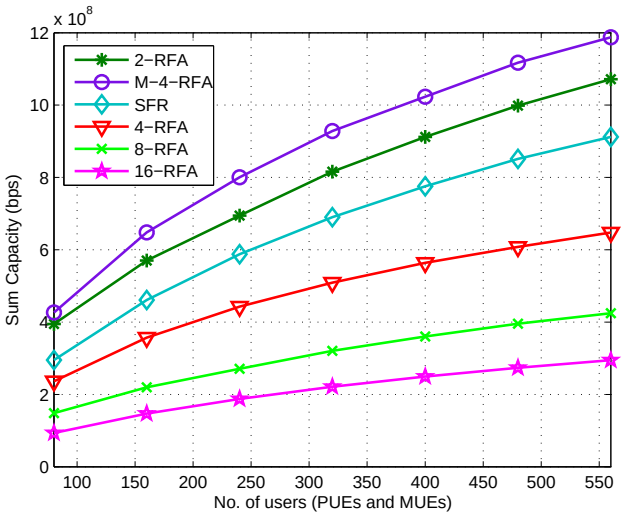


Figure 5.2: Sum-rate capacity analysis for varying number of downlink PUEs in multi-cell.

the point that influence of intercell interference in 2-RFA is much larger than the rest of the RFA schemes. Also the hybrid M-4-RFA scheme has a little greater interference than the regular 4-RFA scheme due to enhanced interfering cells. However, it can also be noticed, as we move to higher region RFA, the gap between outage probability of SC and MC reduces because of increased separation among the users, utilizing same sub-band.

The sum capacity of varying number of users in multi-cell is projected in Fig. 5.2. The gains of proposed scheme in terms of throughput are quite obvious from this figure. It can be observed that the throughput of M-4-RFA scheme is highest among all, as the sources of interference are moved apart, compared to the baseline scheme (2-RFA) that has the highest bandwidth. It is worth mentioning that the proposed modified scheme takes the advantage of 2-RFA and 4-RFA, in terms of bandwidth and partitioning of cells into higher regions, respectively. Moreover, 2-RFA does not provide user fairness,

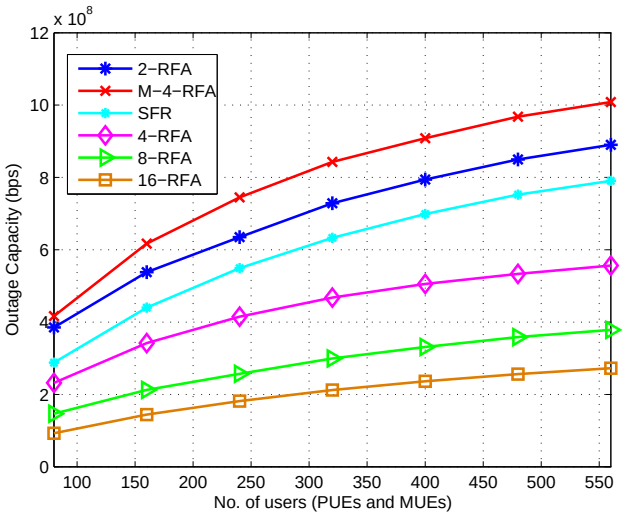


Figure 5.3: Outage capacity of downlink PUEs in multi-cell with increasing user density ( $\beta_1 = 3$, $\beta_2 = 2.5$, $B = 10MHz$).

especially to the cell edge users, as the impact of ICI is severe. Whereas, M-4-RFA scheme does not only provide substantial data rate gains over all the other RFA schemes, in addition, it offers considerate higher rates to the cell edge users.

In Fig. 5.3, we depict the outage capacity, which is defined as the maximum constant rate that is maintained over the fading block for the provided outage probability. The 2-RFA scheme provides channel fairness, as a consequence, the cell edge users do not achieve favorable data rates, whereas M-4-RFA is a scheme that provides fairness to all the users, as the intended PUEs have higher SINR values in addition to better data rates. Eventually, when the performance is evaluated in terms of outage capacity, which depicts the sum rate of the users when they are in coverage instead of ergodic rate, it can be observed that the M-4-RFA provides higher outage capacity as compared to baseline schemes, which validates that even at higher user

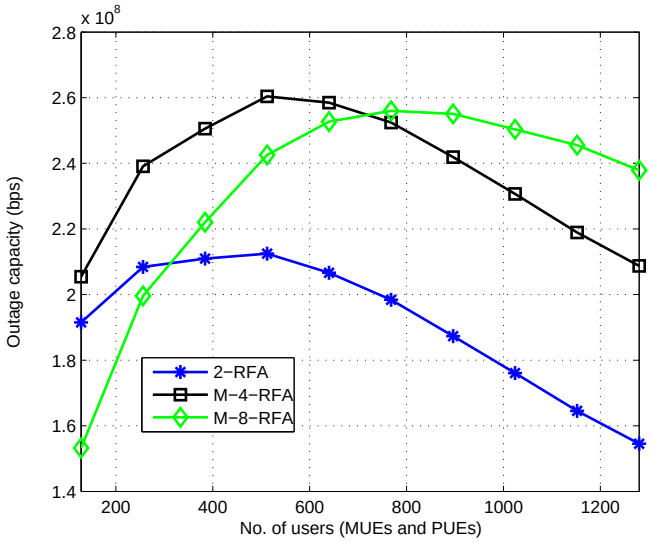


Figure 5.4: Outage capacity comparison of various modified RFA schemes with 2-RFA scheme in multi-cell.

density, hybrid RFA scheme outperforms all the remaining RFA schemes.

The comparison between various M-RFA schemes is given in Fig. 5.4. As it is stated previously, by combining the benefits of different RFA schemes, we can gain better rates. We have compared modified 4 and 8 RFA schemes with the conventional 2-RFA scheme. In order to observe the behavior of prominent interference from the neighboring regions, the radius of macrocells is assumed to be 1 Km. Fig. 5.5 shows that, at a very dense user population, higher region M-RFA schemes show better performance, for example, at user density of 1024, M-8-RFA provides 42.13% gain as compared to 2-RFA and 8.4% higher outage capacity than M-4-RFA. However, this gain is achieved at the cost of higher complexity and challenge of dealing the frequent handoffs. Therefore, we do not need to divide the cell into higher regions, instead M-4-RFA scheme can provide substantial data rates even at a dense number of

users. Thus, it can be concluded that, it is not required to opt for higher region modified RFA schemes, as these schemes provide minimal increase in throughput with much higher resource consumption.

## 5.2 Results & System Performance for analytical expressions

In the previous sections, the analytical expressions for the coverage probability and rate coverage have been derived, whereas the accuracy of these expressions is validated by simulations in this section. To investigate the system performance, two simulation scenarios are considered. In the first case, the location of the PBSs, PUEs and that of MUEs is assumed to be uniformly distributed, whereas the second case follows by modeling the lo-

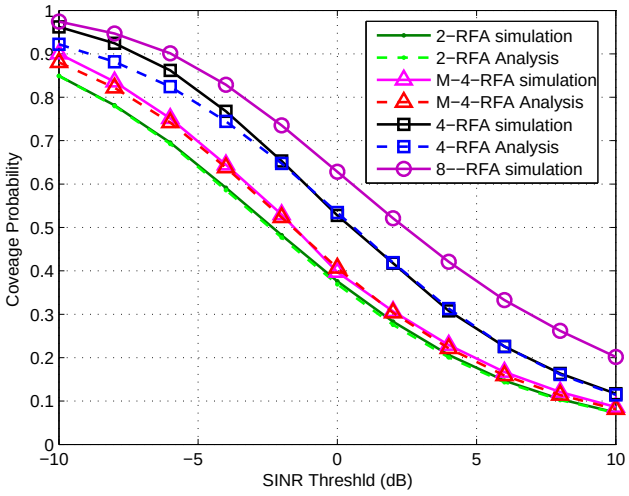


Figure 5.5: Coverage probability comparison of 2, 4, M-4, 8-RFA schemes in a two tier network ($\beta_1 = 3$, $\beta_2 = 2.5$, No noise).

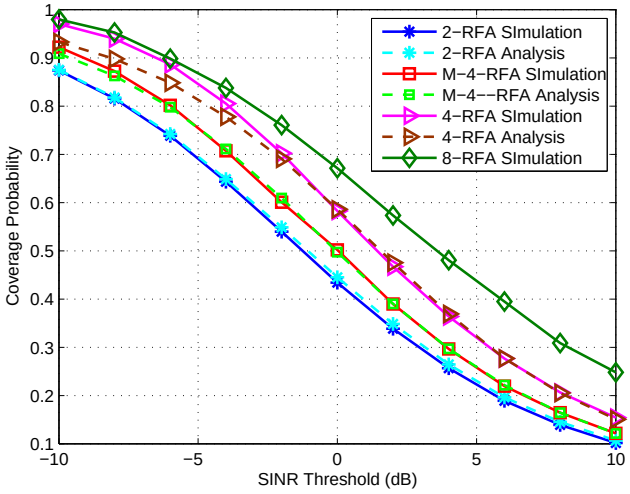


Figure 5.6: Coverage probability comparison of 2, 4, M-4, 8-RFA schemes in a two tier network ($\beta_1 = 3.5$, $\beta_2 = 2.75$, No noise).

cations of PBSs and MUEs as spatial PPPs.

A two tier network is considered, where the radius of macro cell is assumed 1 km and is divided into two regions of equal area for 2-RFA and four regions of equal areas for 4-RFA and M-4-RFA schemes, respectively. The rest of the parameters are shown in Table 5.1. The comparison of three theoretically derived results of 2-RFA, 4-RFA and M-4 and 8-RFA, using fluid model with that of Monte-Carlo simulations is depicted in Fig. 5.5. The path loss exponent for pico cells is taken as 2.5 and that of macro users as 3. It can be noticed that as we divide the macrocell area into regions, the coverage probability increases, i.e, 8-RFA provides best coverage as compared to 4-RFA. Similarly 4-RFA outperforms 2-RFA. The figure also shows that M-4-RFA provides better coverage as compared to 2-RFA when the downlink PUE receives the same amount of interference as in 2-RFA, however these entities are now distantly located, due to modified sub-band allocation. In 4-RFA,

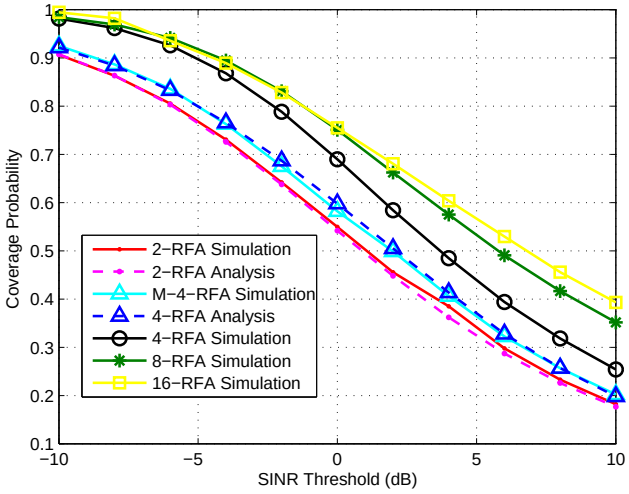


Figure 5.7: Coverage probability comparison of different RFA schemes in a two tier network , ($\beta_1 = 4$, $\beta_2 = 3.5$, $\lambda_2 = 3\lambda_1$, No noise).

users of each region get cross-tier interference from only one region, therefore, a better coverage is obtained, however the users are deprived of higher data rates, due to bandwidth division. Also from the figure, it is validated that the simulation results agree with the trends generated through the analytical expressions for varying SINR threshold. In Fig. 5.6, the path loss exponents of pico tier and that of macro tier is assumed 2.75 and 3.5, respectively. The figure also follows the similar trends in the simulation as well as the numerically computed values as of Fig. 5.5.

In Figs. 5.7 and 5.8, the PBSs are modeled as PPP having intensity $\lambda = 3.8216 \times 10^{-5}\ BSs/m^2$. The values of path loss exponents for the pico cells and macrocell are 3.5 and 4 for Fig. 5.8, whereas 3.75 and 4.5 for Fig. 5.9, respectively. Firstly, the simulation results are quite close to analytical ones. Another fact that can be observed that it is not useful to partition the macrocell into higher regions because after dividing the macrocell into more

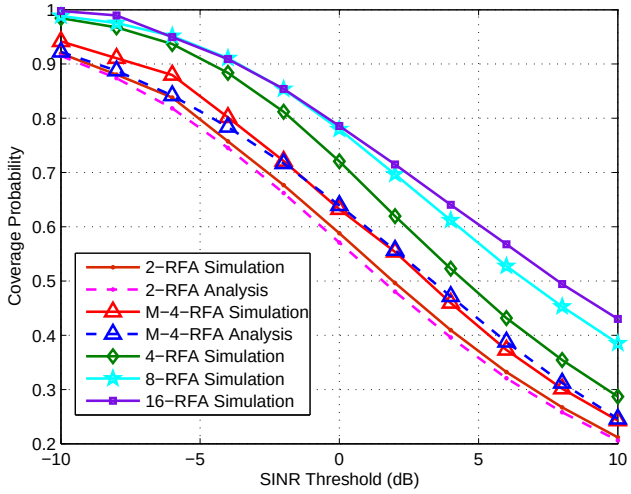


Figure 5.8: Coverage probability comparison of different RFA schemes in a two tier network , ($\beta_1 = 4.5$, $\beta_2 = 3.75$, $\lambda_2 = 3\lambda_1$, No noise).

than 8 regions, saturation occurs and no significant improvement in coverage probability is achieved.

Next the impact of thermal noise on the achievable coverage probability

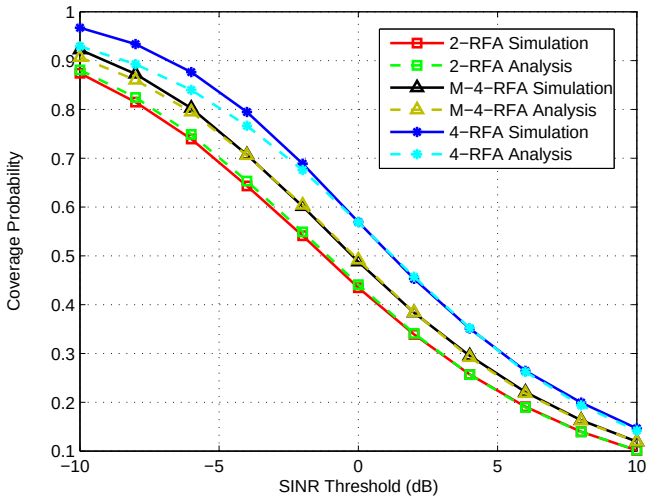


Figure 5.9: Coverage probability comparison of RFA schemes in a two tier network ($\beta_1 = 2.75$, $\beta_2 = 3.5$, noise thermal density = -174 dBm/Hz).

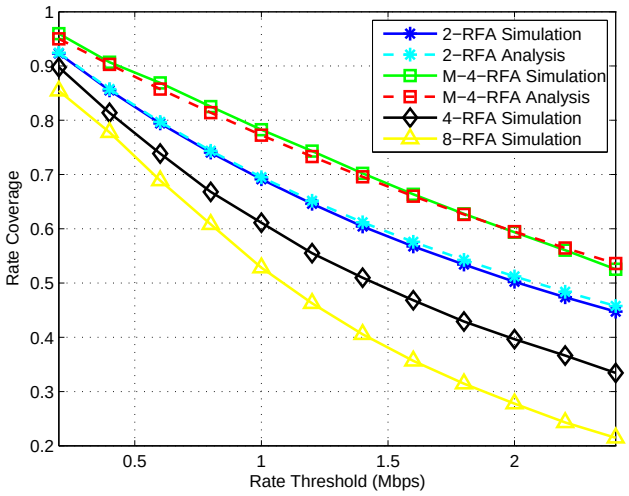


Figure 5.10: Rate coverage comparison between RFA schemes in a two tier network. (The operational system bandwidth is assumed 10 MHz, $\beta_1 = 3.5$, $\beta_2 = 2.75$).

is investigated, the remaining simulation environment remains the same and thermal noise density is taken as -174 dBm/Hz. The result is provided in Fig. 5.9, which verifies the fact that even after including noise the intended downlink users follow the same coverage trend when only interference is considered. For instance, at the SINR threshold value of -6 dB, the coverage probability of users using 2-RFA scheme is affected by 0.08% and that of M-4-RFA by 0.09% with the addition of noise. Hence, this result supports our claim that in the presence of interference, the noise is not an influential factor and thus can be ignored.

The graphs in Figs. 5.10 and 5.11, show rate coverage probabilities, $P(\delta)$, as a function of the rate threshold $\delta$. We can observe that the M-4-RFA shows higher rates as opposed to the 2, 4 and 8-RFA, which is expected given the reduced level of interference and greater bandwidth allotted to users. We can

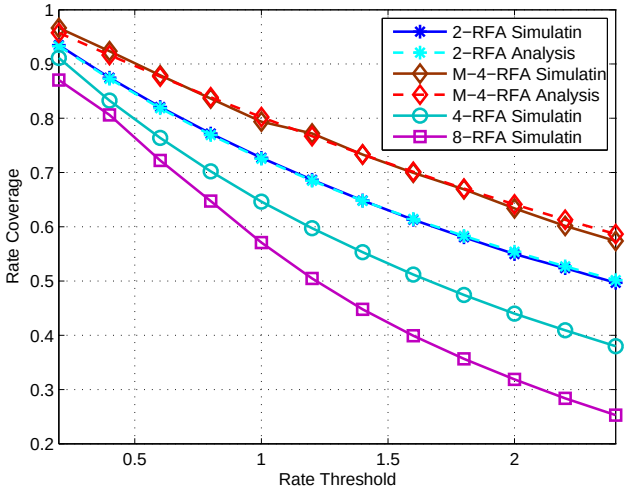


Figure 5.11: Rate coverage comparison between RFA schemes in a two tier network. (The operational system bandwidth is assumed 10 MHz, $\beta_1 = 4$, $\beta_2 = 3$).

also see that the simulation results follow the similar trend generated using Lemma 3.

# Chapter 6

# Conclusion & Future Work

The deployment of heterogeneous networks (Het-Nets) inevitably demands the design of interference management techniques to elevate the overall network performance. For the performance enhancement of DL PUEs, in terms of better coverage, Qos and data rates, in this thesis we presented a novel interference mitigation technique known as reverse frequency allocation (RFA), which provides an efficient resource allocation compared to other state-of-the-art techniques. RFA reverses the transmission direction of interferers, thereby minimizing the cross-tier interference. Eventually, better coverage as well as increased data rates are achieved by providing complementary spectrum to the macro and pico users. We proposed the implementation of a W-region RFA scheme in multi-cellular network to minimize the effect of ICI. Moreover, the performance of the network can be further intensified by combining several RFA schemes into single network to form M-RFA scheme that provides fairness along with improved data rates to the users, in particular, to the cell edge users.

Furthermore, by utilizing stochastic geometry tools, we derived the analytical expressions of coverage probability and rate coverage for various RFA schemes. Our analysis assumes that there is no cross-tier interference from other macro cells and prove that the proposed modified 4-RFA scheme is the optimal scheme among other RFA schemes. Mathematical modeling is performed using two different approaches, in first approach the location of the interferers is modeled as independent PPPs, best suitable for higher values of pathloss exponent. Whereas, in the second approach the expected value of the cumulative interference is calculated implementing fluid model and by applying Jensens inequality lower bound on the coverage probability is evaluated, this model provides accurate results for small path loss exponent values. The plausibility of model is validated through Monte-Carlo simulations and the network performance is evaluated in terms of coverage probability, coverage rate, sum capacity and outage capacity. The performance of the network is evaluated by varying sets of parameters, that validates that despite of a little increased complexity as compared to baseline 2-RFA and SFR scheme, the proposed M-4-RFA scheme provides huge performance gain. It can thus be concluded that M-RFA schemes offer significant margin in outage capacity, which is verified for different user densities as well as by varying the threshold values.

As a future work, the analysis can be extended to the multi cellular network, where in addition the impact of sectoring, addition of antennas, handoff mechanism when users move from one region to another and power allocation schemes can be studied.

# Bibliography

[1] Chen, Shanzhi, and Jian Zhao, "The requirements, challenges, and technologies for 5G of terrestrial mobile telecommunication," *IEEE Commun. Mag.*, pp. 36-43, 2014.

[2] D. Lopez-Perez, I. Guvenc, G. De la Roche, M. Kountouris, , T.Q. Quek, and J. Zhang, "Enhanced intercell interference coordination challenges in heterogeneous networks," *IEEE Wireless Commun.*, vol. 18, no. 3, pp.22-30, 2011.

[3] E. Bjrnson, M. Kountouris, and M. Debbah, "Massive MIMO and small cells: Improving energy efficiency by optimal soft-cell coordination," *IEEE International Conference on Telecommunications (ICT)*, pp. 1-5, 2013.

[4] A. ur Rahman, and S.A. Hassan, "Analysis of composite fading in a single cell downlink cooperative heterogeneous networks," *IEEE Vehicular Technology Conference (VTC Spring)*, pp. 1-5, 2015.

[5] Small Cell Forum. *Small Cell Market Status*, accessed on Jun. 2016. [Online]. Available: http://www.smallcellforum.org/

[6] V. Chandrasekhar, J.G. Andrews, and A. Gatherer, "Femtocell networks: a survey," *IEEE Communications magazine*, pp.59-67, 2008.

[7] A. Damnjanovic, J. Montojo, Y. Wei, T. Ji, T. Luo, M. Vajapeyam, T. Yoo, O. Song, and D. Malladi, , "A survey on 3GPP heterogeneous networks," *IEEE Wireless Commun.*, vol. 18, no. 3, pp.10-21, 2011.

[8] P. vist, and A. Simonsson, "LTE HetNet trial-range expansion including micro/pico indoor coverage survey," *IEEE Veh. Technol. Conference (VTC Fall)*, pp. 1-5, 2012.

[9] S. Mishra, and C.S.R. Murthy, "Femtocells An efficient location aware distributed physical resource block assignment for dense closed access femtocell networks," *Computer Networks Elsevier*, pp.164-175, 15 Jan. 2016.

[10] Y. Yu, M. Peng, J. Li, A. Cheng, C. Wang, "Resource allocation optimization for hybrid access mode in heterogeneous networks," *IEEE Wireless Commun. and Networking Conference (WCNC)*, pp. 1243-1248, Mar. 2015.

[11] S.A. Raza, S.A. Hassan, H.B. Pervaiz, Q. Ni, and L. Musavian, "Self-Adaptive Power Control Mechanism in D2D Enabled Hybrid Cellular Network with mmWave Small Cells: An Optimization Approach" *IEEE GLOBCOM*, 2017.

[12] H. Munir, S. A. Hassan, H. Parveiz, Q. Ni, "A Game Theoretical Network-Assisted User-Centric Design for Resource Allocation in

5G Heterogeneous Networks," *IEEE Vehicular Technology Conference (VTC-Spring)* , May, 2016.

[13] H. Munir, S. A. Hassan, H. B. Parveiz, Leila Musavian, Qiang Ni, "Energy Efficient Resource Allocation in 5G Hybrid Heterogeneous Networks: A Game Theoretic Approach," *IEEE Vehicular Technology Conference (VTC-Fall)*, Sep, 2016.

[14] M.S. Omar, M.A. Anjum, S.A. Hassan, H. Pervaiz, and Q. Niv, "Performance analysis of hybrid 5G cellular networks exploiting mmWave capabilities in suburban areas" *IEEE International Conference on Communications (ICC)*, pp. 1-6, 2016.

[15] S. H. Waqar, and S. A. Hassan, "Fuzzy logic-based downlink subchannel allocation for capacity maximization in OFDMA femtocells," *IEEE Wireless Commun. and Mobile Computing Conference (IWCMC)*, pp. 1073-1078, 2015.

[16] S. Rangan, T.S. Rappaport, and E. Erkip, "Millimeter-wave cellular wireless networks: Potentials and challenges," *Proceedings of the IEEE*, vol. 102, no. 3, pp.366-385, 2014.

[17] J. G. Andrews et al., "What will 5G be?," *IEEE J. Sel. Areas Commun.*, pp. 1065-1082, 2014.

[18] A. Ghosh et al., "Heterogeneous cellular networks: From theory to practice," *IEEE Commun. Mag.*, vol. 50, pp. 54-64, June 2012.

[19] X. Wu, B. Murherjee, and D. Ghosal, "Hierarchical architectures in the third-generation cellular network," *IEEE Trans. Wireless Commun.*, vol. 11, no. 3, pp. 62-71, 2004.

[20] V. Chandrasekhar, J. G. Andrews, and A. Gatherer, "Femtocell networks: A survey," *IEEE Comm. Mag.*, vol. 46, no. 9, pp. 59-67, Sep. 2008.

[21] J. G. Andrews, H. Claussen, M. Dohler, S. Rangan, and M. C. Reed, "Femtocells: Past, present, and future," *IEEE J. Sel. Areas Commun.*, vol. 30, no. 3, pp. 497-508, Apr. 2012.

[22] S. Park, W. Seo, S. Choi and D. Hong, "A beamforming codebook restriction for cross-tier interference coordination in two-tier femtocell networks," *IEEE Trans. Veh. Technol.*, vol. 60, no. 4, pp.1651-1663, 2011.

[23] D. L. Perez, et al, "Enhanced intercell interference coordination challenges in heterogeneous networks," *IEEE Wireless Commun.*, vol. 18, no. 3, pp.22-30, 2011.

[24] M. Peng, K. Zhang, J. Jiang, J. Wang, and W. Wang, "Energy-efficient resource assignment and power allocation in heterogeneous cloud radio access networks," *IEEE Trans. Veh. Technol.*, vol. 64, no. 11, pp.5275-5287, 2015.

[25] Y. Lin, W. Bao, W. Yu, and B. Liang, "Optimizing user association and spectrum allocation in HetNets: A utility perspective," *IEEE J. Sel. Areas Commun.*, vol. 33, no. 6, pp. 1025-1039, 2015.

[26] J. G. Andrews, "Seven ways that HetNets are a cellular paradigm shift," *IEEE Commun. Mag.*, vol. 51, no. 3, pp. 136-144, 2013.

[27] N. Saquib, E. Hossain, and D. Kim., "Fractional frequency reuse for interference management in LTE-advanced hetnets," *IEEE Wireless Commun.*, pp. 113-122, 2013.

[28] S. Singh, H. S. Dhillon, and J. G. Andrews, "Offloading in heterogeneous networks: Modeling, analysis, and design insights," *IEEE Trans. Wireless Commun.*, pp. 2484-2497, 2013.

[29] M. Bennis, M. Simsek, A. Czylwik, W. Saad, S. Valentin, and M. Debbah, "When cellular meets WiFi in wireless small cell networks," *IEEE Commun. Mag.*, pp. 44-50, June 2013.

[30] D. Lopez-Perez, I. Guvenc, G. De La Roche, M. Kountouris, T. Q. Quek, and J. Zhang, "Enhanced intercell interference coordination challenges in heterogeneous networks," *IEEE Wireless Commun.*, vol. 18, pp. 22-30, June 2011.

[31] T. Zahir, K. Arshad, A. Nakata, and K. Moessner, "Interference management in femtocells," *IEEE Commun. Surveys Tutorials*, vol. 15, no. 1, pp. 293-311, 2013.

[32] S. U. Abdullahi, J. Liu, C. Huang, and X. Zhang, "Enhancing throughput performance in LTE-Advanced Hetnets with buffered Fractional Frequency Reuse," *IEEE Ubiquitous and Future Networks (ICUFN)*, pp. 918-923, 2016.

[33] T. D. Novlan, R. K. Ganti, A. Ghosh, J. G. Andrews, "Analytical Evaluation of Fractional Frequency Reuse for Heterogeneous Cellular Networks," *IEEE Trans. Wireless Commun.*, vol. 60, pp. 2029-2039, 2012.

[34] R. Singh, and C. S. R. Murthy, "Techniques for Interference Mitigation Using Cooperative Resource Partitioning in Multitier LTE HetNets," *IEEE Systems Journal*, pp. 1-11, Feb. 2016.

[35] D. Muirhead, M. Imran, and K. Arshad, "A Survey of the Challenges, Opportunities and Use of Multiple Antennas in Current and Future 5G Small Cell Base Stations," *IEEE Access*, vol. 4, pp. 2952 - 2964, May 2016.

[36] R. Zahid, and S. A. Hassan, "On the performance of multiple region reverse frequency allocation scheme in a single cell downlink heterogeneous networks," *IEEE Wireless Commun. and Mobile Computing Conference (IWCMC)*, pp. 387-392, August 2014.

[37] M. Z. Chowdhury, Y. M. Jang, and Z. J. Haas, "Cost-effective frequency planning for capacity enhancement of femtocellular networks," *Wireless Personal Commun.*, vol. 60, Issue 1, pp. 83-104, Sept. 2011.

[38] Simsek, M., M. Bennis, and Czylwik, "Dynamic inter-cell interference coordination in HetNets: A reinforcement learning approach," *IEEE Global Communications Conference (GLOBECOM)*, pp. 5446-5450,2012.

[39] N. Saquib, E. Hossain, and D. Kim., "Fractional frequency reuse for interference management in LTE-advanced hetnets," IEEE Wireless Commun., pp. 113-122, 2013.

[40] Abderrazak, J. B., and H. Besbes, "A tailored fractional frequency reuse scheme for Heterogeneous Networks," *IEEE International Wireless Commun. and Mobile Computing Conference (IWCMC)*, pp. 419-424, 2015.

[41] P. Jacob, A. S. Madhukumar, A. P. Vinod, "Handling interference in self-organizing femtocell networks through frequency-polarization diversity," *Wireless Networks-Springer Journal*, pp. 383-401, 2016.

[42] P. Jacob, A. James, and A. S. Madhukumar, "Interference mitigation through reverse frequency allocation in multi-tier cellular network: a downlink perspective," *Wireless Networks*, pp. 1613-1629, July 2015.

[43] H. B. Chang, and I. Rubin, "Optimal downlink and uplink fractional frequency reuse in cellular wireless networks," *IEEE Trans. Veh. Technol.*, no. 4, pp. 2295-2308, 2016.

[44] A. Ijaz, S. A. Hassan, D. N. K. Jayakody, "A Multiple Region Reverse Frequency Allocation Scheme for Downlink Capacity Enhancement in 5G HetNets" *IEEE Consumer Communications Networking Conference (CCNC)*, 2017.

[45] J. G. Andrews, F. Baccelli, and R. K. Ganti, "A tractable approach to coverage and rate in cellular networks," *IEEE Trans. on Commun.*, pp. 3122-3134, 2011.

[46] R. Zahid, and S. A. Hassan, "Stochastic Geometry-based Analysis of Multiple Region Reverse Frequency Allocation Scheme in Downlink HetNets," *IEEE Wireless Commun. and Mobile Computing Conference (IWCMC)*, pp. 1289-1294, August 2015.

[47] H. Zhang, S. Chen, L. Feng, Y. Xie, and L. Hanzo, "A universal approach to coverage probability and throughput analysis for cellular networks," *IEEE Trans. Veh. Technol.*, no. 9, pp. 4245-4256, 2015.

[48] J. M. Kelif, M. Coupechoux, and P. Godlewski, "A fluid model for performance analysis in cellular networks," *EURASIP J. Wireless Commun. Netw.*, vol. 2010, pp. 1-11, Aug. 2010.

[49] S. Singh, H.S. Dhillon, and J.G Andrews, "Offloading in heterogeneous networks: Modeling, analysis, and design insights," *IEEE Trans Wireless Commun.*, vol. 12, no. 5, pp.2484-2497, May 2013.